

## Global buckling of S690 transversely-stiffened plate girders with slender webs: Behaviour and design

Item Type	Journal article
Authors	Zhang, YM;Hassanein, MF;Bock, M;Shao, YB
Citation	Zhang, Y., Hassanein, M.F., Bock, M. and Shao, Y. (2021) Global buckling of S690 transversely-stiffened plate girders with slender webs: Behaviour and design. <i>Thin-Walled Structures</i> , 161, 107519.
DOI	<a href="https://doi.org/10.1016/j.tws.2021.107519">10.1016/j.tws.2021.107519</a>
Publisher	Elsevier
Journal	Thin-Walled Structures
Download date	2026-05-20 20:02:26
License	<a href="https://creativecommons.org/licenses/by-nc-nd/4.0/">https://creativecommons.org/licenses/by-nc-nd/4.0/</a>
Link to Item	<a href="http://hdl.handle.net/2436/624059">http://hdl.handle.net/2436/624059</a>

# GLOBAL BUCKLING OF S690 TRANSVERSELY-STIFFENED PLATE GIRDERS WITH SLENDER WEBS: BEHAVIOUR AND DESIGN

YU-MEI ZHANG<sup>1</sup>, M. F. HASSANEIN<sup>1,2,\*</sup>, MARINA BOCK<sup>3</sup>, YONG-BO SHAO<sup>1</sup>

<sup>1</sup>*School of Civil Engineering and Geomatics, Southwest Petroleum University, Chengdu, Sichuan, PR China, 610500*

<sup>2</sup>*Department of Structural Engineering, Faculty of Engineering, Tanta University, Tanta, Egypt*

<sup>3</sup>*School of Architecture and Built Environment, Faculty of Science and Engineering, University of Wolverhampton, Wolverhampton WV1 1LY, United Kingdom*

*\*Corresponding author.*

E-mail address: [yumei\\_zhang@163.com](mailto:yumei_zhang@163.com) (Y.M. Zhang), [mostafa.fahmi@f-eng.tanta.edu.eg](mailto:mostafa.fahmi@f-eng.tanta.edu.eg) (M.F. Hassanein), [Marina.Bock@wlv.ac.uk](mailto:Marina.Bock@wlv.ac.uk) (Marina Bock), [ybshao@swpu.edu.cn](mailto:ybshao@swpu.edu.cn) (Y.B. Shao)

## ABSTRACT

High-strength steels (HSSs) are now used globally in different structural applications because of their constructional and environmental merits. Though, investigations on HSS elements are still relatively limited. Herein, the lateral-torsional buckling (LTB) response of laterally-unsupported plate girders with stiffened slender webs is explored considering steel S690, which is currently under extensive testing worldwide. This is done by the finite element (FE) modelling to provide numerical models that well simulate their actual behaviour. Accordingly, the FE models are verified first through comparisons with available tests in the literature. After that, parametric analyses are generated to examine the effects of the geometrical characteristics of the cross-section (in terms of the effective radius of gyration for LTB ( $r_T$ ) and the elastic section modulus referred to compression flange ( $S_{xc}$ )) and the laterally-unsupported length on the behaviour and strength of these girders. The results show that by increasing the value of  $r_T$ , computed as the radius of gyration about the minor-axis of the compression flange plus one-sixth of the web, the strength of the girders increase more efficiently compared with the relative increase in  $r_T$ . On the other hand, while increasing the

value of the section modulus  $S_{xc}$  is found to raise the strength of the girders, the increase in the strength has been relatively found to be less than the increase in the value of  $S_{xc}$ . Additionally, based on the current results, the girder slenderness parameter of 2.0 is found as the inelastic LTB limit of such girders built up with S690, from which the girders of larger slenderness become ineffective and better to be made of conventional normal-strength steels. Furthermore, the bending strengths are compared with the design models given by AISC, EC3-1-1 and AS4100. The results show that they provide highly conservative results, with the predictions of AS4100 yielding the best design values. However, enhancements to the design models are still possible to provide lighter girders under the same applied loads. Accordingly, EC3 general design model (provided in Clause 6.3.2.2) is modified by using buckling curve "a" instead of buckling curve "d".

**KEYWORDS:** Lateral-torsional buckling; Transversely-stiffened web; Radius of gyration, Elastic section modulus, HSS; S690; Finite element; Design; Buckling curve.

## 1. INTRODUCTION

### 1.1 Advantages of high strength steels

Currently, structural steel grades are becoming much higher than before due to the development in steel material technologies accompanied by the need to design lighter and more slender structures. Hence, the term of “high strength steel (HSS)” becomes familiar nowadays in the construction sector. HSSs are considered as those steels having a minimum yield/proof stress ( $f_y$ ) of  $460\text{MPa}$ . Recently, they have increasingly been used in different structural engineering applications [1-3]. This is because they offer attractive structural solution to heavily-loaded girders and columns owing to their high strength-to-weight ratio.

Moreover, compared with conventional normal-strength steels (NSSs), the application of HSS reduces the overall material consumption as well as the carbon dioxide emission in steel and building industries [4-5]. For global development, steel is used in large quantities in structural applications and with the fast growth of towns, such as the New Capital of Egypt and Chengdu of China, the need for the structural steel becomes greater. At present, gas emissions and energy consumptions are the major environmental concerns with steel production [5]. According to the World Steel Association [6], utilising HSSs instead of NSSs reduces the steel material total release of 0.156 billion tons CO<sub>2</sub> equivalents. Therefore, using HSS in construction becomes crucial to save the environment by effectively reducing the carbon dioxide releases from steel production process. Accordingly, the literature shows that a considerable research has recently been directed to investigate the fundamental behaviour of different steel elements formed from S690; see for examples Refs. [7-11]. Practically, S690 is available in different forms in the markets, with plates of different thicknesses being existed. Additionally, steel S690 has excellent forming and welding characteristics [3]. So, nowadays different cross-sections of steel S690 can easily be manufactured to fit with several structural applications [1-4].

## **1.2 Lateral-torsional buckling of transversely-stiffened plate girders**

Traditionally, bridges and long-span girders are formed from built-up I-section girders (IPGs). Logically, with the increase in the clear span of these girders, their depths have to increase to withstand the large vertical deflections. This results in the use of thin-walled steel plates. Accordingly, these girders become susceptible to flexural-torsional buckling failure modes with web distortion [12]. Moreover, slender webs fail prematurely under shear loads [13]. Additionally, the webs may locally buckle under the large concentrated loads, causing the girder to fail by crippling [14]. Accordingly, such heavily-loaded girders with slender

webs are usually stiffened transversely; see Fig. 1 which represents a practical use of such girders at the Southwest Petroleum University in China. The literature reveals that the web distortion is often eliminated [15] and both the shear [16] and patch loading strengths [17] are enhanced by using these stiffened webs.



**Fig. 1:** Application of plate girders with stiffened webs in the laboratory of SWPU

On the other hand, one of the main possible failure modes of the IPGs with stiffened slender webs, under consideration in this investigation, is the lateral-torsional buckling (LTB). This failure mode takes place in the relatively long girders, because the overall slenderness of the girder increases compared with the web slenderness. In Fig. 2 [18], the buckling and failure modes of a typical long IPG are presented. Clearly, the buckling mode has merely lateral displacement, whereas the failure mode possesses both lateral displacement and major-axis downward deflection. Accordingly, the buckling mode is mainly depending on the lateral stiffness of the cross-section, which in turn is affected by the radius of gyration about the minor-axis of the compression flange. On the opposite, the failure mode is influenced by both the radius of gyration of the compression flange and the section modulus.

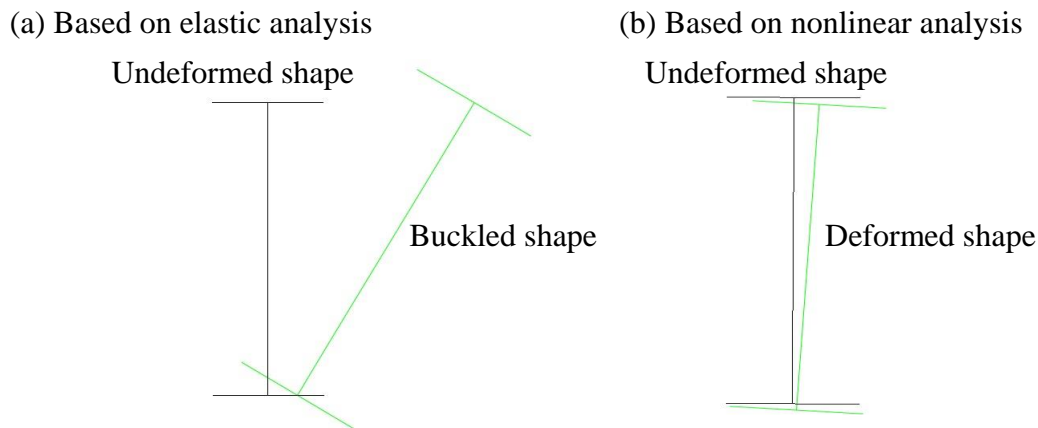


**Fig. 2:** Buckled/deformed and undeformed shapes for a typical transversely-stiffened IPG [18]

### 1.3 Problem statement

Recently, Bradford and Liu [19] studied *numerically* the LTB strength of HSS IPGs; concentrating on those girders formed from steel S960. They indicated that design methods implemented in international specifications are not accurate enough to predict the strengths of such girders. Consequently, they modified these design methods by fitting the results of the numerical analysis. This highlights the significance of exploring the behaviour of members formed from HSSs because current design formulae are based on testing NSS members. To the authors' best knowledge, this failure mode has not been addressed before for IPGs made of steel S690, despite such girders were utilised to erect a 20m-span bridge in Mttådalen, Sweden. Hence, this paper is delivered to focus on girders made of such steel grade through finite element (FE) modelling, from which ABAQUS program was used to execute this investigation. Note that despite the previous experiences of the current research group on studying LTB behaviour of advanced homogenous [18, 20] and hybrid [21] girders by using the FE modelling, additional verifications on conventional I-section girders have been added in this paper. Nevertheless, the material model of steel S690, which will be used in the FE modelling of the current IPGs, should be verified first. This is presented in the next section, which is followed by the verifications of the LTB of the laterally-unrestrained girders.

## 2. APPROPRIATE MATERIAL MODEL FOR S690

### 2.1 General

Herein, the test specimens of Sun, et al. [8] were used to find the appropriate material model that well mimic the actual behaviour of steel S690, in order for the currently considered IPGs to be simulated properly. They experimentally studied [8] the major-axis bending moment resistances and behaviour of short beams under four-point bending. All specimens (named as I- $h \times b_f \times t$ ; where  $h$ ,  $b_f$ ,  $t$  are the depth, flange width and thickness of the flanges and web elements, respectively) were fabricated by welding hot-rolled plates of S690 HSS taken from the same batch of 5mm thick. The measured dimensions of the six test specimens [8] are presently given in Table 1, where  $L$  is the length of the beams.

**Table 1:** Measured geometrical properties [8] and predicted strengths of the specimens used for material model validation

Specimen ID	$L$ [mm]	$h$ [mm]	$b_f$ [mm]	$t$ [mm]	$M_{ul,FE}$ [kN·m]	$\frac{M_{ul,FE}}{M_{ul,Exp}}$
I-50x50x5	495.7	49.44	49.42	4.97	9.5	0.95
I-70x70x5	696.5	67.15	69.29	4.93	18.2	0.94
I-80x60x5	693.7	79.39	59.01	4.96	20.3	0.97
I-90x70x5	698.1	90.35	69.20	4.93	26.8	0.97
I-100x100x5	998.5	99.02	99.09	4.91	39.0	0.98
I-140x70x5	1397.3	139.33	69.23	4.94	48.1	0.97
<b>Average</b>						<b>0.96</b>
<b>Standard deviation</b>						<b>0.016</b>

Generally, to virtually test the FE models considering both geometric and material nonlinearities, an initial elastic run of the model should be performed to essentially obtain the buckling shape. This buckling shape is used as the imperfect shape of the girder, as can be seen later. In the current validation, the maximum imperfection was used as  $t/100$ , where  $t$  is the measured plates' thickness, based on the imperfection analyses [8] for the short specimens which failed by local

plate buckling. As for the residual stresses, Sun, et al. [8] noticed their insignificant effects on the specimens. So, their effects were currently neglected.

## **2.2 Load application, boundary conditions and mesh type**

In this subsection, the applied load and boundary conditions of the test specimens of Sun et al. [8] are firstly described, followed by the mesh type. In these tests, the constant bending moment (BM) distribution was applied by using the four-point bending. Herein, the applied loads and boundary conditions used in the validation are shown in Fig. 3. As can be noticed, there are four cross-sections assigned in each model to set the boundary conditions easily, including two sections at the end supports and a section at each loading point. The two end supports were located at 50 mm from each end section and the two load points were located at the span's third points of all girders. Herein, a reference point (RP) located at the intersection of the web and the bottom flange at each end support section was created. Then, the section of each end support was coupled to the corresponding RP. Both RPs were allowed to rotate about the same bending axis, while only one RP was allowed to move longitudinally. Because two G-clamps were placed during testing [8] to eliminate any LTB, further lateral and torsional constraints were added to FE model to develop the same effect. Each cross-section of the loading points was also coupled to the corresponding RP which is located at the intersection of the web and the top flange. These two RPs were allowed to rotate about the bending axis and to translate in the axial and vertical directions. It is worth to mention that the constraints of the two loading points adopted only in 'Step-1' of the nonlinear analyses. With respect to load application, displacement control mode was applied to the nonlinear static Riks analyses in FE model, as shown by the two red arrows in Fig. 3. On the other hand, the shell element S4R was employed to simulate the transversely-stiffened IPGs, which owns four nodes and considers the reduced integration.

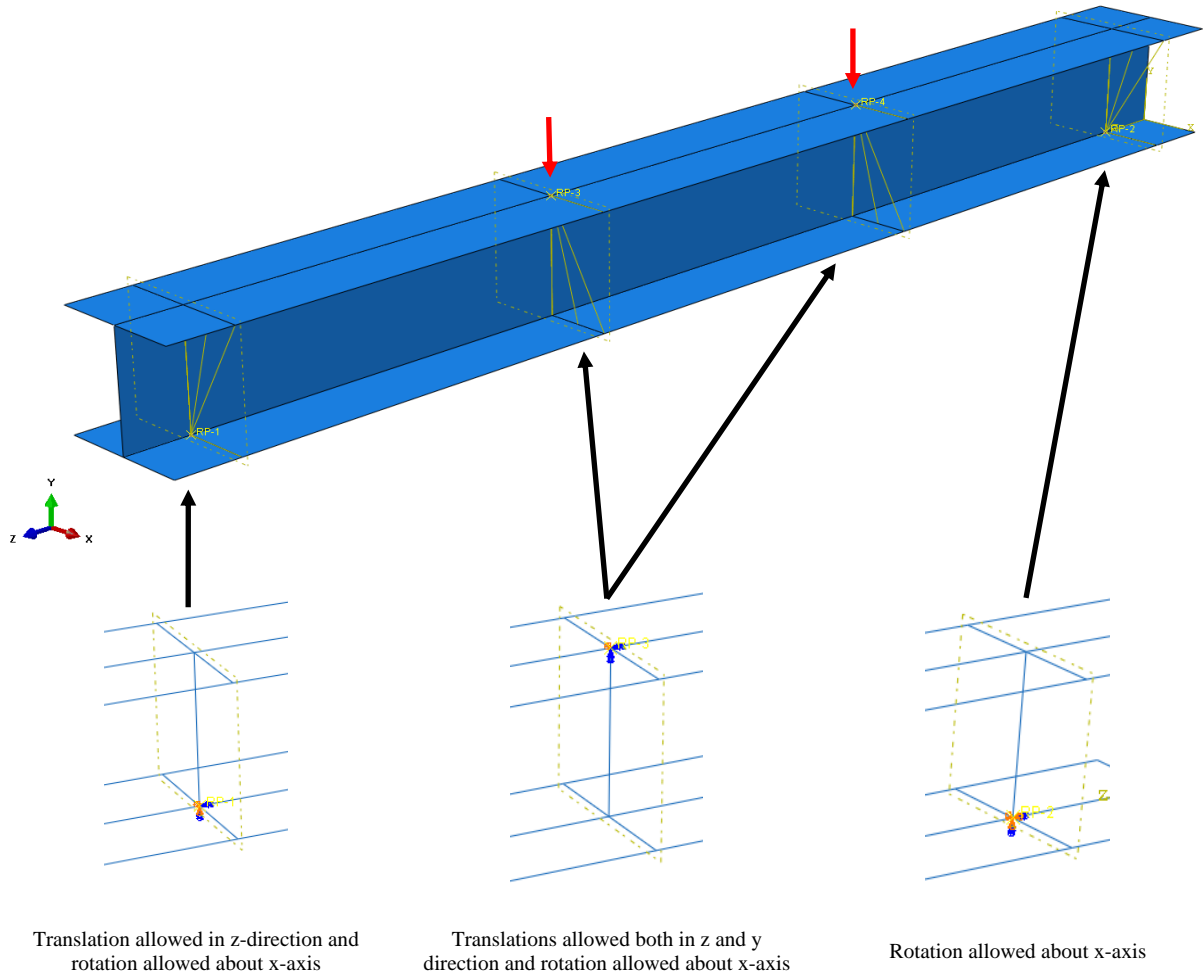


**Fig. 3:** Loading and boundary conditions of the short S690 beams [8]

## 2.3 Material modelling and validation

### 2.3.1 Description of material model

Previously, three stress-strain models (Fig. 4) were suggested in the literature to simulate the HSS material behaviour [20]. Among them, the elastic-plastic with strain hardening relationship (Fig. 4(a)) has been used to simulate the experimental tests of Sun, et al. [8] made of S690. The Von Mises yield criterion was assigned to simulate the HSS behaviour, which considers the isotropic hardening rule. According to the tensile test results of Sun, et al. [8], the S690 HSS has a yield stress of 702.6 MPa and an ultimate strength of 750.3 MPa, while the strain at the ultimate stress ( $\epsilon_u$ ) was 11%. The elastic modulus ( $E$ ) is 216000 MPa and the Poisson's ratio was assigned a value of 0.3, which has been used extensively in FE

simulations in the literature. It should be noted that the tested material properties were used in the current investigation of the transversely-stiffened IPGs. Moreover, the analyses were run by using the true stresses ( $\delta_{true}$ ) and plastic strains ( $\varepsilon_{true}^{pl}$ ) [22-23] converted from the measured stresses and strains, respectively, as can be calculated by Eqs. (1) and (2):

$$\delta_{true} = \delta(1 + \varepsilon) \quad (1)$$

$$\varepsilon_{true}^{pl} = \ln(1 + \varepsilon) - \frac{\delta_{true}}{E_0} \quad (2)$$

where  $\delta$ ,  $\varepsilon$  and  $E_0$  represent, respectively, the measured stress, strain and Young's modulus.

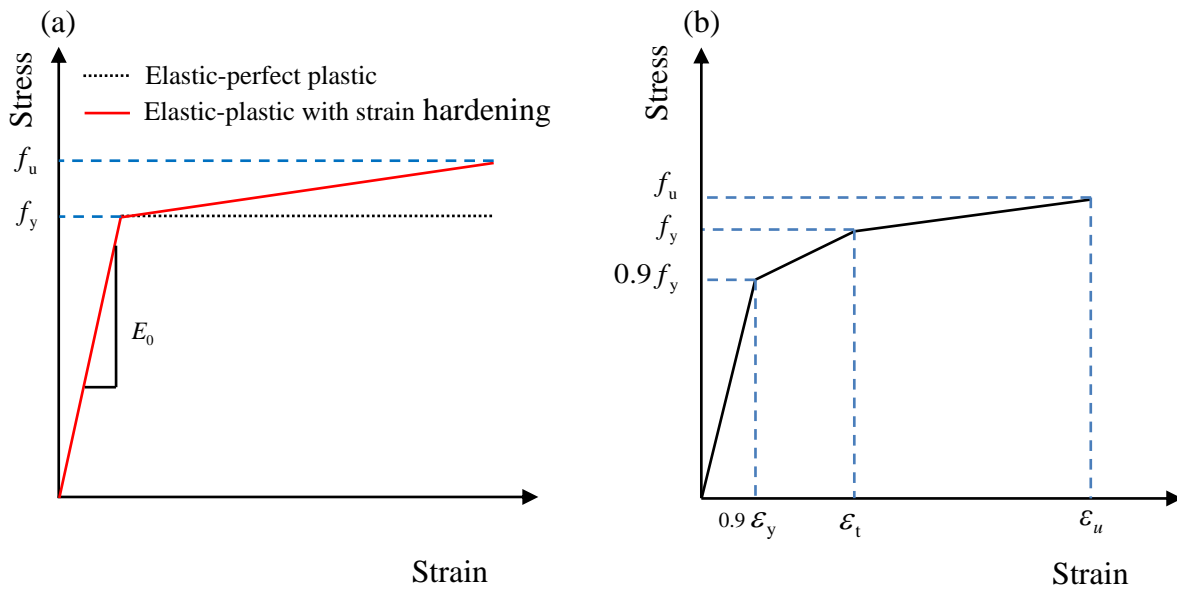


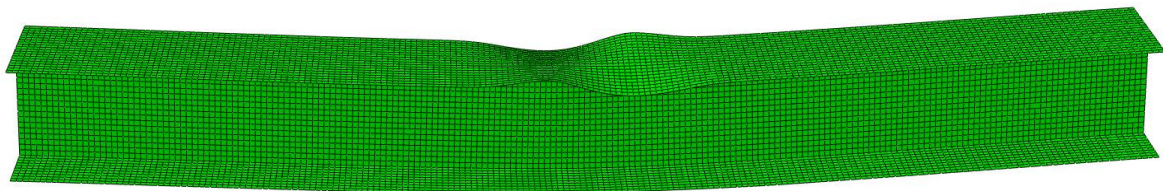
**Fig. 4:** Stress-strain relationships for HSSs using (a) bi-linear and (b) tri-linear curves

### 2.3.2 Verification of the material model

In this subsection, the comparison between the FE models and the experimental results of Sun, et al. [8] is presented. As can be noticed, the failure mode obtained from FE modelling (Fig. 5(a)) typically represents the test failure mode of Sun, et al. [8] for the specimen I-100x100x5. This

was obtained by considering the lowest positive eigenmode shown in Fig. 5(b), as discussed earlier. The predicted bending moment strengths ( $M_{ul,FE}$ ), obtained from FE modelling, have been used to calculate the relative FE-to-experiment strengths as given in Table 1. From this table, the FE modelling seems to provide good estimations for the ultimate bending moments, with an average ratio of 0.96 for the FE-to-experimental strengths ( $M_{ul,FE}/M_{ul,Exp}$ ) and a very low standard deviation of 0.016. Additionally, the comparisons between the FE modelling and experimental [8] normalised moment ( $M/M_{pl}$ )-curvature ( $k/k_{pl}$ ) relationships of the specimens are presented in Fig. 6. As can be realised from this figure, the FE modelling predicts well the relative moment-curvature relationships of the specimens. From above comparisons, it can be ensured that the considered material model (i.e. the elastic-plastic with strain hardening relationship) for steel S690 is accurate and can be used in further analyses, as made in the next sections.

(a) FE failure mode (obtained from nonlinear analysis)



(b) FE buckling mode (obtained from elastic analysis)

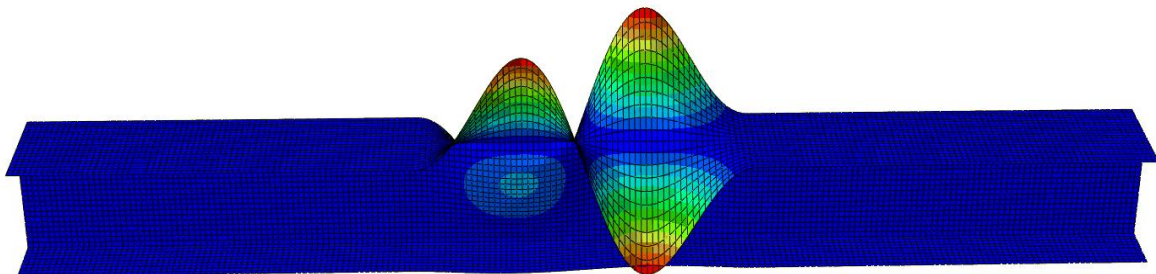


**Fig. 5:** Typical FE (a) failure and (b) buckling modes for specimen I-100x100x5

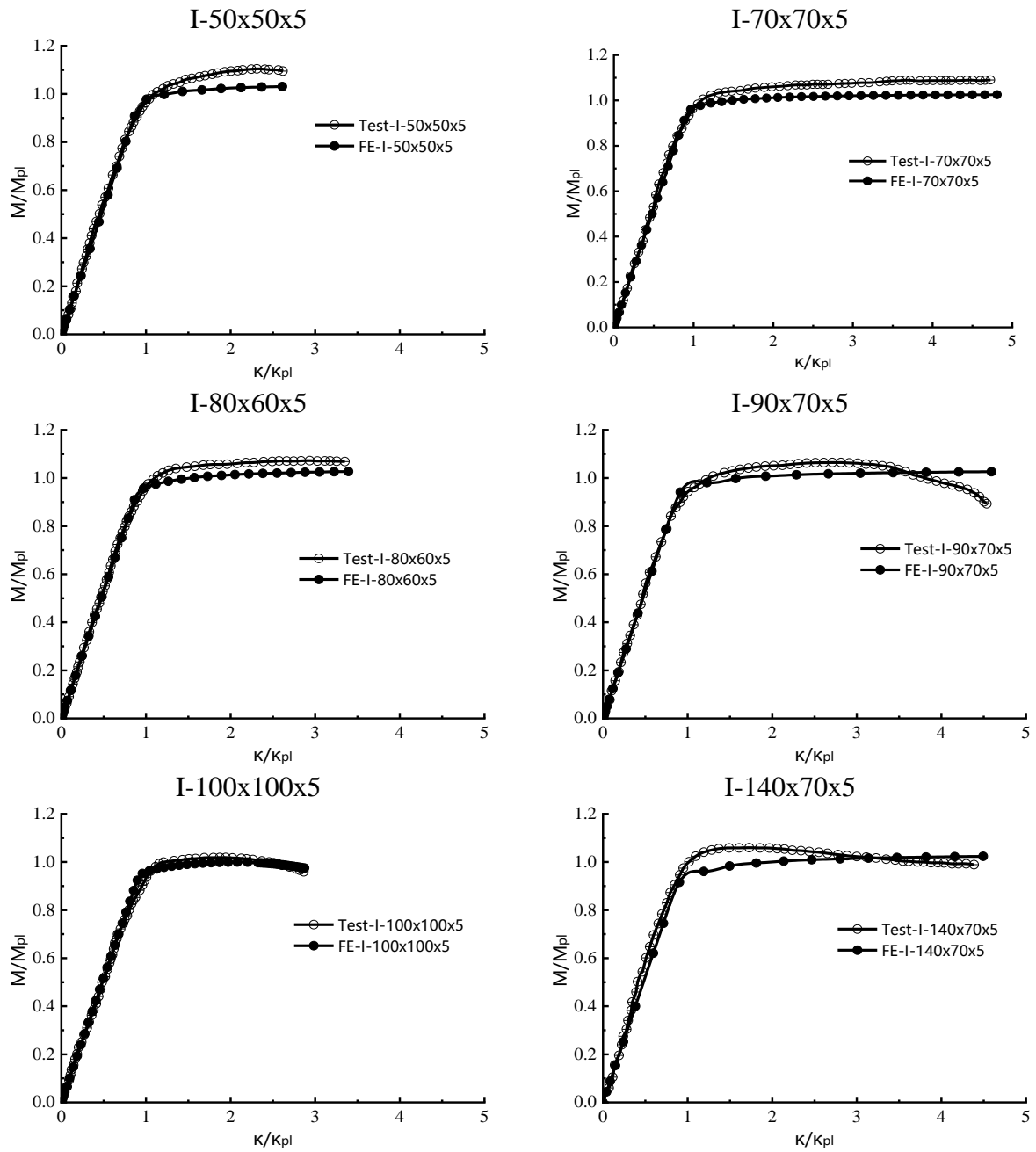


**Fig. 6:** Comparison between experimental [8] and FE modelling normalised moment-curvature relationships for the specimens built up from S690

### 3. DESCRIPTION OF IPGS NUMERICAL MODELS

#### 3.1 General

As can be noticed from the Introduction, girders failing by LTB have been numerically validated and investigated by this research group in Refs. [18, 20-21]. However, the current

increasing trend of designing by advanced analyses, as a new standard is developing in Europe to design by FE analysis [24], prompted the authors to discuss each single detail related to the current IPGs. As stated earlier, the current paper investigates the IPGs with transversely-stiffened slender webs which are formed from steel S690. The girders are simply supported and loaded by constant BM. This is the most critical loading condition used by codes as the reference to other less severe varying BM situations. An imperfection value of  $L/1000$  [25-26], which scales the global buckling mode captured from the lowest positive eigenmode of the buckling analysis, was used in investigating the IPGs, where  $L$  is the span of the girder. This is equal to 75% of the fabrication tolerance recommended as  $L/750$  for steel global buckling by EN1090-2 [27]. Additionally, as the effects of residual stresses were found negligible for transversely-stiffened IPGs with slender webs [22-23, 28-29], they were neglected in this investigation. In the following, the description of current girders is given in detail.

The entire FE models were simulated with simple supports at both end sections and the details are presented clearly in Fig. 7. It should be noticed that all girders were simulated by using non-rigid end posts [30] with the supports located at distances of  $h_w/10$  from both ends of the girders; where  $h_w$  is the web depth. Both supports of each girder were considered rollers, and in order to maintain the stability of the girder, a point at web-to-bottom flange juncture at the centre line of the girder was restrained in the axial direction. Based on preliminary FE analyses, the restriction of the rotation about z-axis at the end supports was found to be insignificant as long as the web is laterally restrained. However, they were applied in the current FE models. With regard to the loading, the constant BM of each girder was applied by two force couples at both end sections. To do so, the intersection line of each flange with the web at the end support was coupled to a RP located at its mid-point. Then, the concentrated forces were applied at these four RPs, with directions suitable to generate the

two force couples, as presented by the four red arrows in Fig. 7. To verify the loading and boundary conditions of the current girders, eigenvalue buckling analysis was adopted to obtain the buckled shape and eigenvalue for the models used in the present parametric analyses (Section 4). A typical example of the buckled shape is given in Fig. 8, which ensures that the LTB took place for the current transversely-stiffened IPGs. With respect to the critical FE moments ( $M_{cr,FE}$ ), the average ratio of the critical FE results to the theoretical values according to Timoshenko and Gere [31] ( $M_{cr,LTB}$ , called hereafter as  $M_{cr,T}$ ) is 1.04 with a standard deviation of 0.019. Fig. 9 shows the critical FE ( $M_{cr,FE}$ ) and theoretical [31] ( $M_{cr,T}$ ) values presented against  $\lambda$  which is the slenderness of the girders (computed as the square root of the yield-to-critical bending moments), where the results well confirm the accuracy of the loading and boundary conditions of the current transversely-stiffened IPGs.

### 3.2 Meshing

The shell element S4R was employed herein to simulate the transversely-stiffened IPGs, which owns four nodes and considers the reduced integration. Considering the running time and the accuracy of results, additional meshing analysis was executed to select the best reasonable mesh size. Fig. 10(a) provides that the relationship between the mesh size varying from 10mm to 130mm (with an increment of 5mm) and the ratio of  $M_{cr,FE} / M_{cr,T}$ . The effect of mesh size on the running time was also explored as shown in Fig. 10(b). Based on above analyses, a mesh size of 50mm was utilised in further parametric analyses, from which Fig. 11 shows a typical meshed shape of the current FE model.

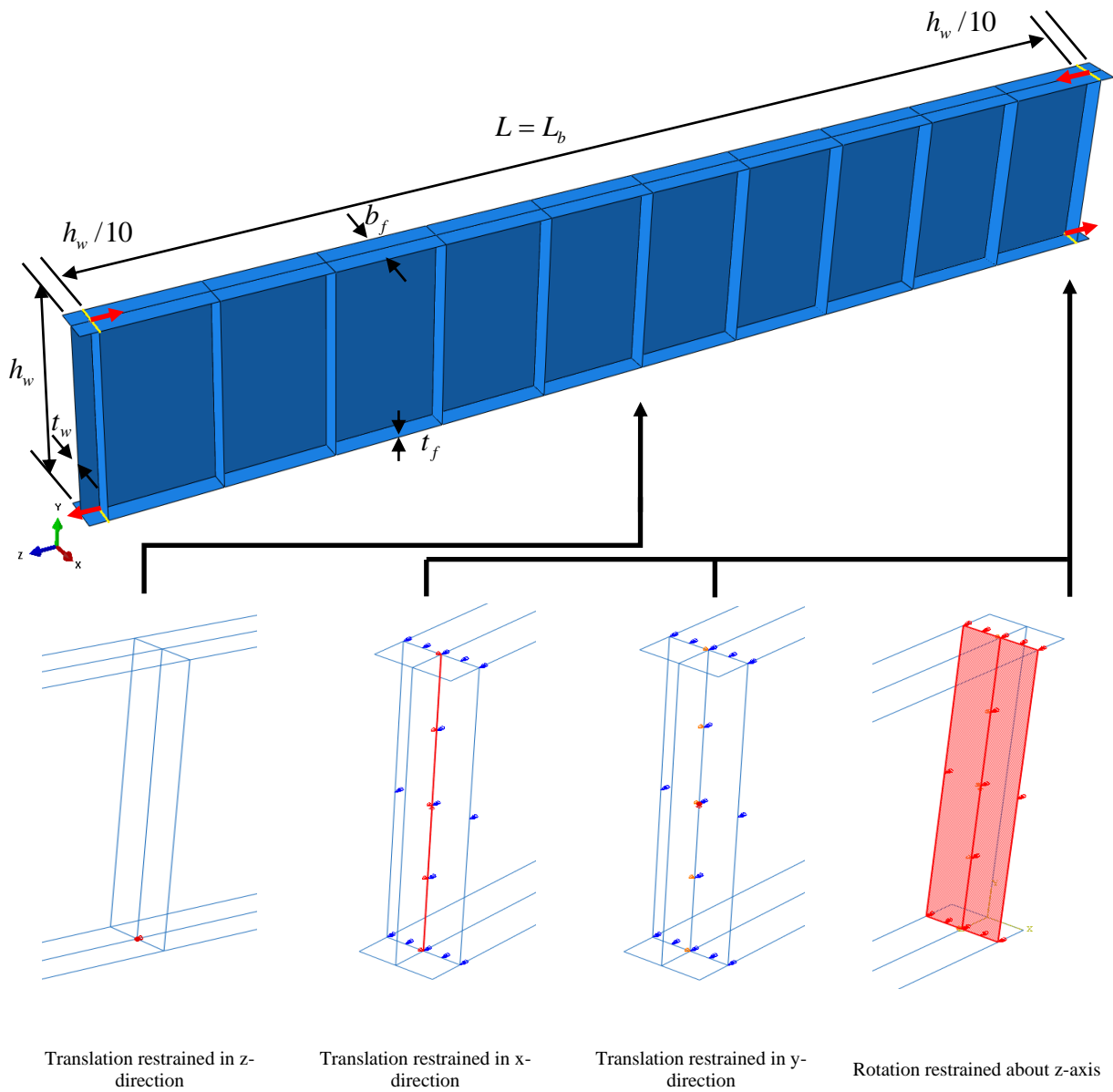


**Fig. 7:** Loading and boundary conditions of a typical transversely-stiffened IPG

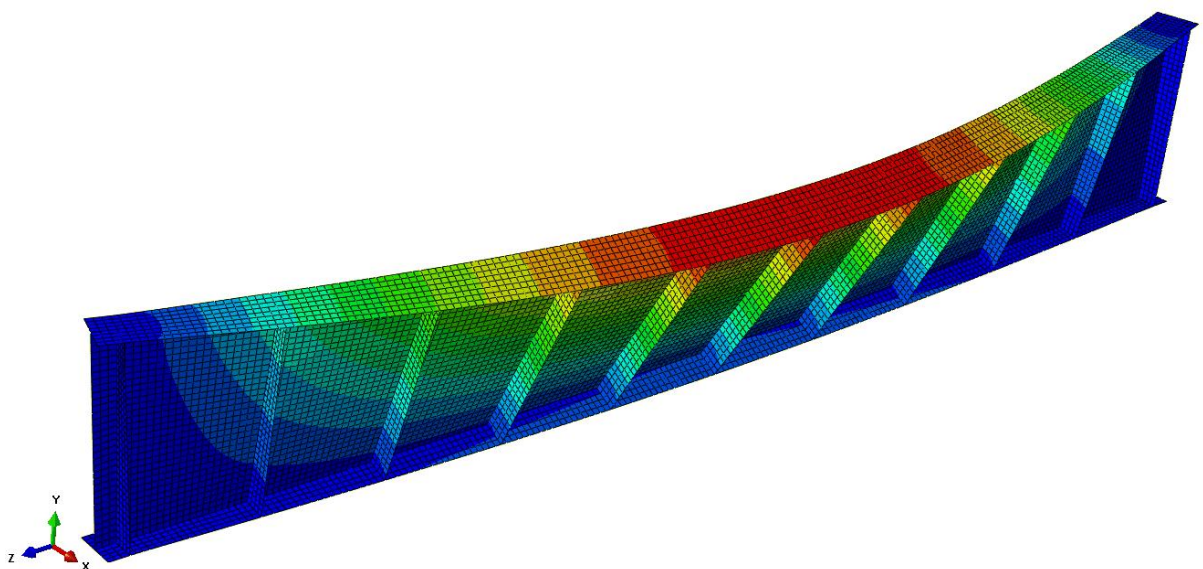


**Fig. 8:** LTB mode of a typical transversely-stiffened IPG

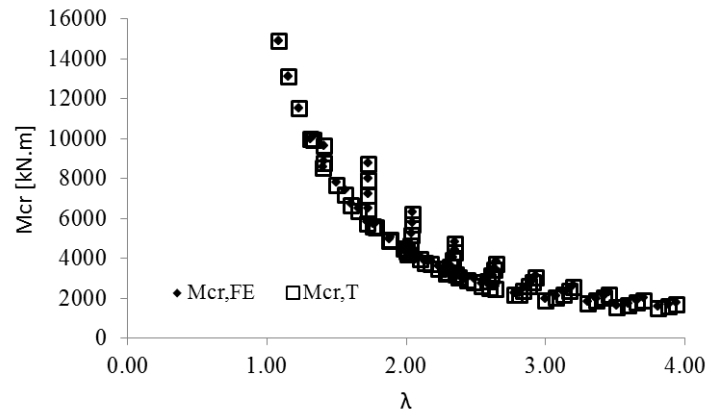


**Fig. 9:** Comparisons between the critical FE and theoretical [31] bending moments

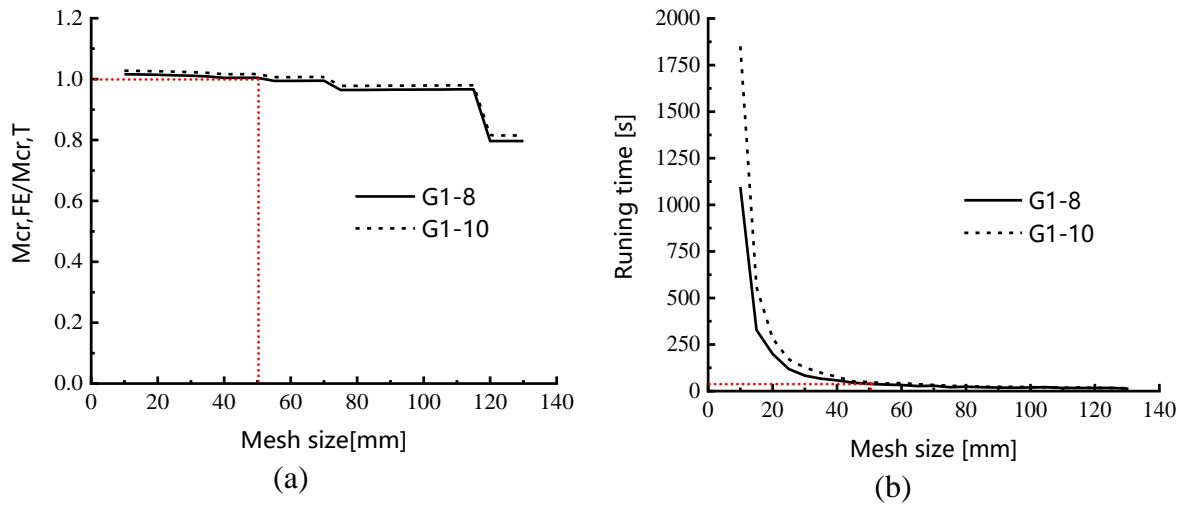


**Fig. 10:** Effect of mesh size on (a) the FE-to-theoretical critical bending moment ratio and (b) the running time

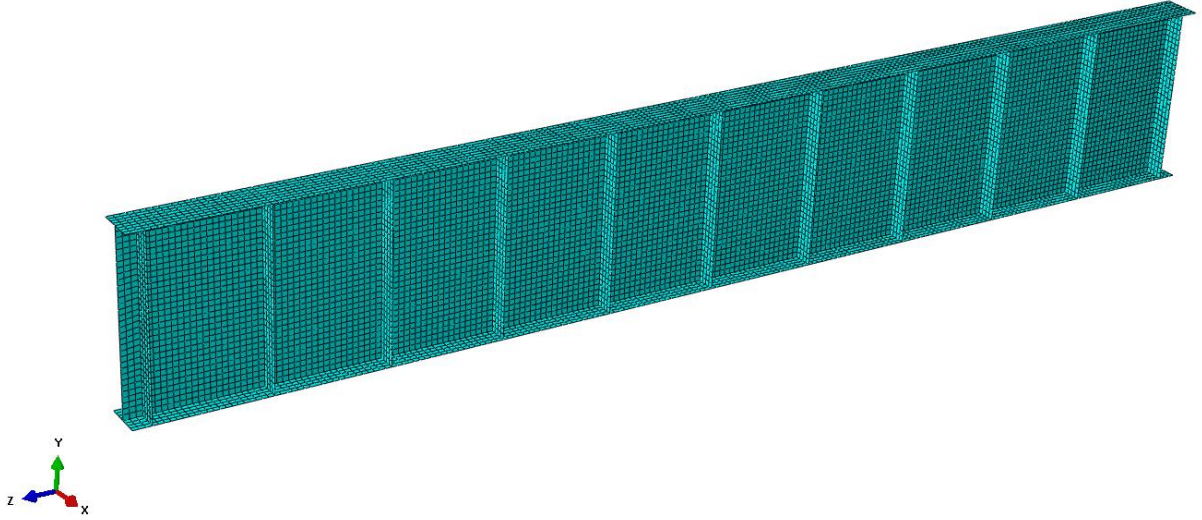


**Fig. 11:** FE mesh of a typical stiffened IPG

### 3.3 Additional validation of LTB failure mode

Despite that accurate verifications have been made by this research group to their FE models failing by LTB in their previous investigations to homogenous [18, 20] and hybrid [21] girders of different cross-sections, additional validation has been added in this subsection. This considers the test specimens of Dibley [32] and Dux and Kitipornchai [33]. These studies investigated experimentally the flexural strength of hot-rolled I-section beams under uniform bending. Herein, the geometrical and material details of the considered beams are given in Table 2, alongside with their experimental ultimate moment strengths ( $M_{ul,Exp}$ ) and the relative FE strengths ( $M_{ul,FE}/M_{ul,Exp}$ ). Note that as the ultimate material strengths were not measured [32-33], the verification considered the elastic-plastic stress-strain material model without strain hardening (similar assumption was considered by Bradford and Liu [19]). This definitely should lead to a conservative modelling. As can be noticed, the average of the  $M_{ul,FE}/M_{ul,Exp}$  ratios is 0.93 (in the safe side) with a standard deviation of 0.013. Hence, this proves that the current FE models can exhibit well the LTB mode. However, the slight conservatism in the FE prediction may, additionally, be attributed to the difficulty of the test setups [32-33] to produce simply supported beams under uniform BMs, which has

also noticed by Bradford and Liu [19] in their valuable FE investigation. Overall, this validation besides those already executed by the authors previously [18, 20-21] prove the suitability of the current FE model to be used in further parametric studies.

**Table 2:** Measured geometrical and material properties [32-33] and predicted strengths of the specimens used for the nonlinear LTB validation

Ref.	Specimen ID	$L$ [mm]	$E$ [MPa]	$f_y$ [MPa]	$M_{ul,FE}$ [kN·m]	$\frac{M_{ul,FE}}{M_{ul,Exp}}$
[32]	8×5.25UB17	2956	203000	505	38.90	0.95
[32]	12×4 UB19	2303	206000	516	118.50	0.93
[32]	12×4 UB19	2639	206000	516	96.80	0.92
[33]	250 UB 37	2500	210000	303	134.63	0.93
<b>Average</b>						<b>0.93</b>
<b>Standard deviation</b>						<b>0.013</b>

## 4. PARAMETRIC STUDIES

### 4.1 Stiffeners arrangement

Currently, the LTB is the main focus of this research. Hence, the deformation of the slender webs, which may lead to the lateral-distortional buckling mode, should be eliminated from the present parametric study. According to White and Jung [34], girders with web panels of  $a/h_w \leq 3.0$  (where  $a$  and  $h_w$  are the web panel length and web depth, respectively) and failing by LTB do not require attaching additional transverse stiffeners for the web to have adequate shear strength. As a known fact [35], stiffeners should be added to the IPGs to develop the required shear strength. Nevertheless, the laterally-unsupported lengths of the girders in practical bridge applications are much less than their span lengths due to the use of cross-girders and/or cross-frames. Consequently, the shear buckling of the slender webs of the IPGs becomes of great importance. Accordingly, smaller web panels should be used to increase the shear buckling strength. Based on this discussion, double-sided out-standing

plate stiffeners, with a thickness of 25.4 mm and attached to the web and flanges of the IPGs, were used in this investigation to produce web panels of  $a/h_w \leq 1.0$ .

## 4.2 Cross-section selection

Parametric studies for the IPGs are carefully designed in this subsection based on three key parameters; namely (1) the effective radius of gyration for LTB ( $r_T$ ), computed as the radius of gyration of the compression flange plus one-sixth of the web following ANSI/AISC 360-16 [35], (2) the elastic section modulus referred to compression flange ( $S_{xc}$ ) and the laterally-unsupported length ( $L_b$ ). These parameters were selected based on the practical design experience of the current authors in addition to the careful examination of the design model presented by AISC [35]. Accordingly, nine groups (G1-G9) have been generated to investigate the above mentioned parameters. The cross-sectional dimensions of Group 1 (G1) models were selected at the beginning considering compact flanges ( $b_f = 350\text{mm}$  and  $t_f = 40\text{mm}$ ) and slender webs ( $h_w = 1600\text{mm}$  and  $t_w = 10\text{mm}$ ) according to the classification system of EC3 [36]. According to Sun, et al. [8], the present slenderness limits classifying the plate elements and the cross-sectional flexural strengths [36] of welded I-sections formed from HSS S690 were found *conservatively* to be safe. Currently, the flanges' slenderness ranged from 0.73 to 0.95 of class 2 limit [36] ( $10 \cdot \sqrt{235 / f_y}$ ), while the webs' slenderness ranged from 1.84 to 3.35 of class 3 limit [36] ( $124 \cdot \sqrt{235 / f_y}$ ). Particularly, all girders had flanges of Class 1, except G5 (having  $b_f$  of 450mm) which was formed from Class 2 flanges. However, the webs, as can be noticed, are too slender compared with class 3 limit of the EC3 [36]. This is to guarantee that the webs are surely slender in nature, as Sun, et al. [8] found that the current class 3 limit for the case of internal compression parts subjected to bending

(i.e. representing the webs of IPGs) specified by EC3 [36] is *highly conservative*. Then, numerical models formed from G1 were conducted to check the failure modes within the selected lengths of  $L_b$ , which extended from 8m to 20m (with an increment of 2m). Actually, girders with lengths of 4m and 6m were generated, but they were found to fail by local buckling. Hence, they were eliminated from the interpretation of the results. The effective radius of gyration for LTB ( $r_T$ ) and the elastic section modulus referred to compression flange ( $S_{xc}$ ) were then calculated and they were equal to  $r_T = 92.6mm$  and  $S_{xc} = 26481270 mm^3$ , respectively. The philosophy of the paper was to examine two main variables (according to AISC [35] specifications), namely (1)  $r_T$  using groups G1-G5 and (2)  $S_{xc}$  via groups G1 and G6-G9. Hence, to generate the girders of groups G2-G5, the flange width ( $b_f$ ) was increased to 375mm (G2), 400mm (G3), 425mm (G4) and 450mm (G5). The web depth ( $h_w$ ) was then computed for each group to obtain *nearly* the same section modulus of group G1 (with a maximum difference of 0.2% found between G3 and G1); see the absolute values of  $S_{xc}$  in Table 3. On the other hand, to get the appropriate dimensions for the girders of groups G6-G9, the web depths ( $h_w$ ) were directly selected as 1800, 2000, 2200 and 2400mm, respectively, with minor changes made to  $b_f$  values to keep the value of  $r_T$  similar to that of G1. Regarding the cross-sectional areas ( $A$ ), it can be noticed that increasing the value of  $S_{xc}$  significantly raises the value of  $A$ , while increasing  $r_T$  does not.

Based upon the previous variables, the study includes girders with web depth-to-flange width ( $h_w / b_f$ ) ratios ranging from 3.0 to 4.5, while the web-to-flange thickness ( $t_w / t_f$ ) ratio was kept constant at 0.25. The flange outstand slenderness was on the range of 4.25 and 5.50. Meanwhile, web plate slenderness varied between 132 and 240. Note that the flange

thickness of 40mm was considered in the whole investigation to eliminate the "*thickness effect*" of the steel material from the current FE models, so that the *nominal* yield stress of steel S690 as specified by EC3 [37] could be used. This is because the yield stresses of steel plates of thicknesses larger than 40 mm are less than the *nominal* value [37]. Note that the material properties of the short tests of Sun et al. [8] were used in these parametric analyses. The details of the groups are summarised in Table 3, from which  $M_y$  represents the cross-sectional elastic (yield) moment. Henceforward, the girders are labelled by their group number and length (in m). For example, "G5-10" describes a girder of Group 5 with a laterally-unsupported length of 10m. Note that all girders of Table 3 had lengths from 8 to 20m to ensure that they are all buckle/fail by LTB which are the main focus of this paper. As given in next section, girders with lengths less than 8m were found to buckle/fail by local buckling. Accordingly, short girders with 4 and 6m, not included in Table 3, were preliminary simulated just for buckling/failure mode comparisons with those girders failing by LTB. On the other hand, it is important to compare between the behaviour and strength of girders formed from S690 and NSS. So, girders of groups G1, G5 and G9 of Table 3 were rerun by considering steel grade S355 [36], which is considered as the most produced and used steel worldwide. Accordingly, groups G1' ( $M_y = 8815 kN \cdot m$ ), G5' ( $M_y = 9148 kN \cdot m$ ) and G9' ( $M_y = 13611 kN \cdot m$ ) have been generated for girders of S355.

**Table 3:** Details of the FE models of the parametric studies – Grey cells stand for the reference group

Group	$b_f$ [mm]	$t_f$ [mm]	$t_w$ [mm]	$h_w$ [mm]	$h_w/t_w$	$A$ [mm <sup>2</sup> ]	$r_T$ [mm]	$S_{xc}$ [mm <sup>3</sup> ]	$L_b$ [m]	$M_y$ [kN·m]
Effect of $r_T$										
<b>G1</b>	<b>350</b>	<b>40</b>	<b>10</b>	<b>1600</b>	<b>160</b>	<b>30000</b>	<b>92.6</b>	<b>26481270</b>	<b>8 – 20</b>	<b>16877</b>
G2	375	40	10	1520	152	30200	<b>100.1</b>	26478133	8 – 20	17099
G3	400	40	10	1450	145	30500	<b>107.6</b>	26543252	8 – 20	17330
G4	425	40	10	1380	138	30800	<b>115.1</b>	26484922	8 – 20	17466
G5	450	40	10	1320	132	31200	<b>122.6</b>	26525486	8 – 20	17637

Effect of $S_{xc}$										
<b>G1</b>	<b>350</b>	<b>40</b>	<b>10</b>	<b>1600</b>	<b>160</b>	<b>30000</b>	<b>92.6</b>	<b>26481270</b>	<b>8 – 20</b>	<b>16877</b>
G6	353	40	10	1800	180	32120	92.6	<b>30602235</b>	8 – 24	19121
G7	356	40	10	2000	200	34240	92.5	<b>34904862</b>	10 – 26	21397
G8	359	40	10	2200	220	36360	92.5	<b>39389062</b>	10 – 28	23704
G9	362	40	10	2400	240	38480	92.5	<b>44054778</b>	10 – 28	26044

## 5. FE RESULTS AND DISCUSSION

### 5.1 Comparison between IPGs formed from HSS and NSS

This subsection compares between the strength and behaviour of IPGs formed from S690 and NSS S355. **Table 4** provides the flexural strengths of the girders of the different grades. Firstly, it is clear from the table that girders formed from S690 exhibit higher strengths compared with those formed from S355. The strength, as can be noticed, is highest for the girders of short laterally unsupported lengths; which are expected to fail inelastically. On the opposite, relatively long girders do not seem to benefit largely from using S690. Accordingly, this highlights the importance of finding a limit differentiating between elastic and inelastic buckling for girders formed from S690, as will be shown later. On the other hand, with respect to the relative  $M_{ul,FE}/M_y$  ratios, it is clear that girders formed from S690 had relatively lower ratios. Hence, a very cost-effective solution is to utilise the HSS “hybrid girders”, which are defined as those girders with flanges of HSS and webs of lower steel grade. This is planned to be done in further publication. Meanwhile, with respect to shear, the webs mostly benefit from increasing the grade of the steel material used; especially in cases of girders laterally-stiffened within short lengths. This again highlights the importance of investigating the IPGs formed from HSS, as they have already been used globally [21].

**Table 4:** Flexural strengths of girders with different material grades

Groups	$L$ [m]	$\lambda$	$M_{ul,FE}$ [kN·m]		[3]/[4]	$\frac{M_{ul,FE}}{M_y}$	
			S690	S355		S690	S355
	[1]	[2]	[3]	[4]	[5]	[6]	[7]
G1 & G1'	8	1.41	7873	6433	1.22	0.47	0.73
	10	1.72	5472	4840	1.13	0.32	0.55
	12	2.01	4094	3735	1.10	0.24	0.42
	14	2.28	3284	2999	1.09	0.19	0.34
	16	2.54	2750	2504	1.10	0.16	0.28
	18	2.78	2322	2166	1.07	0.14	0.25
	20	3.00	2012	1946	1.03	0.12	0.22
G5 & G5'	8	1.09	12673	8316	1.52	0.72	0.91
	10	1.33	9273	7179	1.29	0.53	0.78
	12	1.56	7079	5950	1.19	0.40	0.65
	14	1.78	5731	4929	1.16	0.32	0.54
	16	1.98	4848	4169	1.16	0.27	0.46
	18	2.18	4027	3629	1.11	0.23	0.40
	20	2.35	3517	3279	1.07	0.20	0.36
G9 & G9'	10	1.72	12673	7304	1.11	0.31	0.54
	12	2.04	9273	5456	1.06	0.22	0.40
	14	2.35	7079	4213	1.04	0.17	0.31
	16	2.64	5731	3353	1.03	0.13	0.25
	18	2.93	4848	2746	1.03	0.11	0.20
	20	3.20	4027	2312	1.03	0.09	0.17

On the other hand, the load-deflection relationships for some selected girders are shown in Fig. 12. The deflection was recorded at the mid-span of the girders' lower flanges. In Fig. 12, girders with different lengths of G1 and G1' are considered. Within each selected length (8 and 14m), it can be noticed that characteristics of the curves are almost similar. Generally, it could be observed that the elastic stages of IPGs of different steel grades are coincided, while the change is obvious beyond the ultimate loads. As can be noticed, the failure stage (i.e. pre-peak stage) becomes relatively steeper in case of S355 IPGs compared with S690 IPGs. To the authors, this might be attributed to the fact that S355 IPGs fail at higher  $M_{ul,FE} / M_y$  ratios compared with those of S690 IPGs, hence their failure becomes relatively steeper. Additionally, the deflection corresponding to the ultimate load is much higher for IPGs of S690 compared with those of S355. While this provides a merit for the girders formed from S690, their allowable deflection at the ultimate limit state should be checked properly during design.

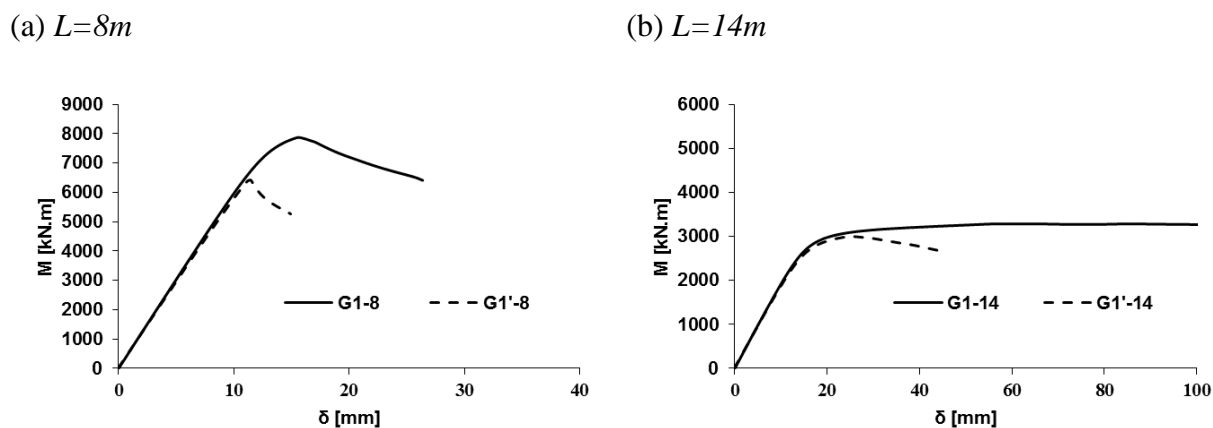


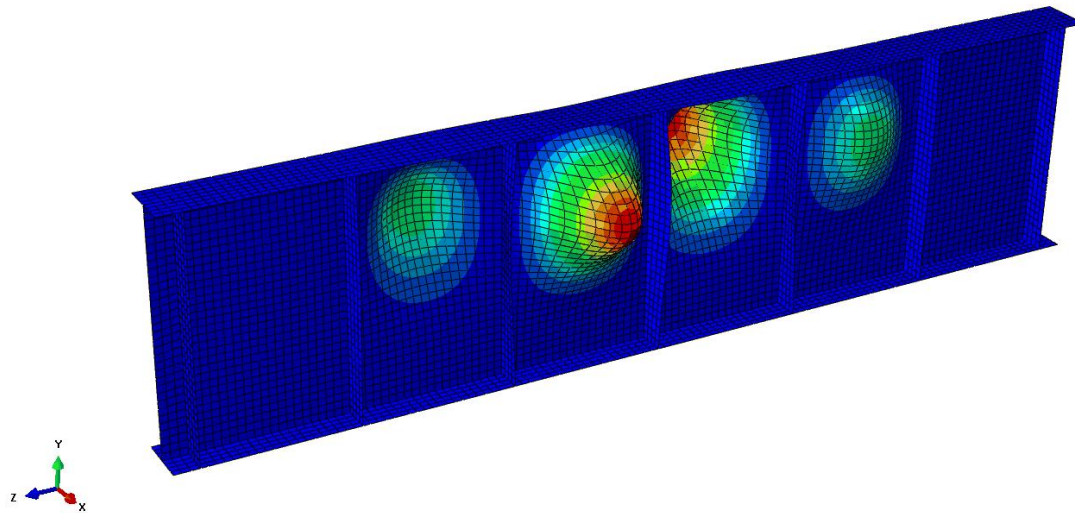
**Fig. 12:** Bending moment-deflection responses of sample IPGs formed from S690 and S355

## 5.2 Fundamental behaviour of IPGs formed from S690

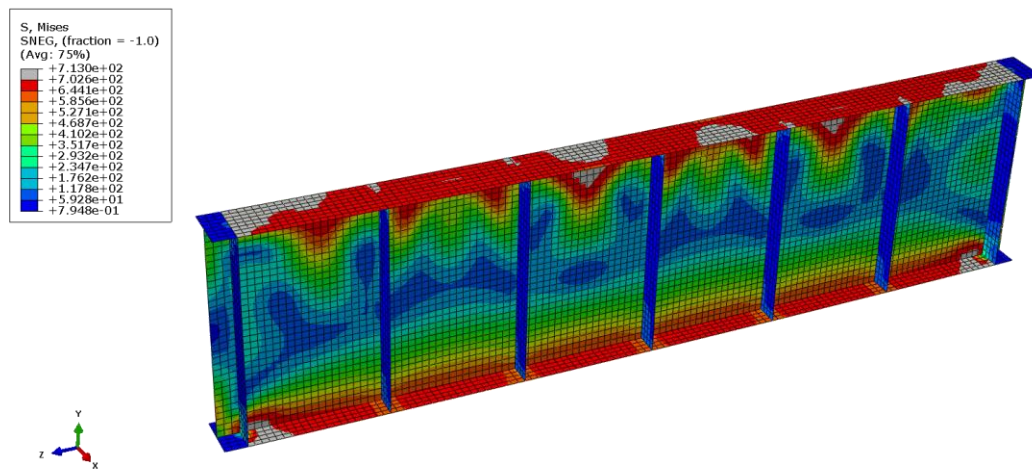
In the preliminary analyses, girders with laterally-unsupported lengths ( $L_b$ ) of 4 and 6m were considered. However, these short girders (despite being laterally-unrestrained) failed by local buckling (LB). The buckling and deformed shapes of a sample girder (that of 6m and belongs to G1) are presented in Fig. 13, from which it can be recognised that short girders exhibit LB of the upper portion of the slender web accompanied by a compression flange twist. No distortion for the cross-section took place as the intersection line between the flange and the web has not displaced from its original position. On the opposite, girders with larger  $L_b$  values failed by LTB. These girders, with  $L_b \geq 8.0m$ , failed by LTB because the girder's slenderness increases and the flanges become more slender compared with the web, and the web distortion was eliminated because of the sufficient attached stiffeners; see Fig. 14. Herein, two LTB have been observed in the results; inelastic LTB and elastic LTB modes. The later failure mode was observed for very long girders which approximately have slenderness parameter over 2.0, as can be seen in Fig. 15 which displays the relationship between  $M_{cr,FE} / M_{ul,FE}$  and the slenderness ( $\lambda$ ). Note that this inelastic limit was based on the

results of groups G1-G5, as all girders of groups G6-G9 were found to fail inelastically based on their maximum considered  $L_b$  values. Hence, additional verification on this limit should be undertaken in future.

(a) Buckling eigenmode



(b) Stress contour captured at ultimate load



(c) Deformed shape at the ultimate load

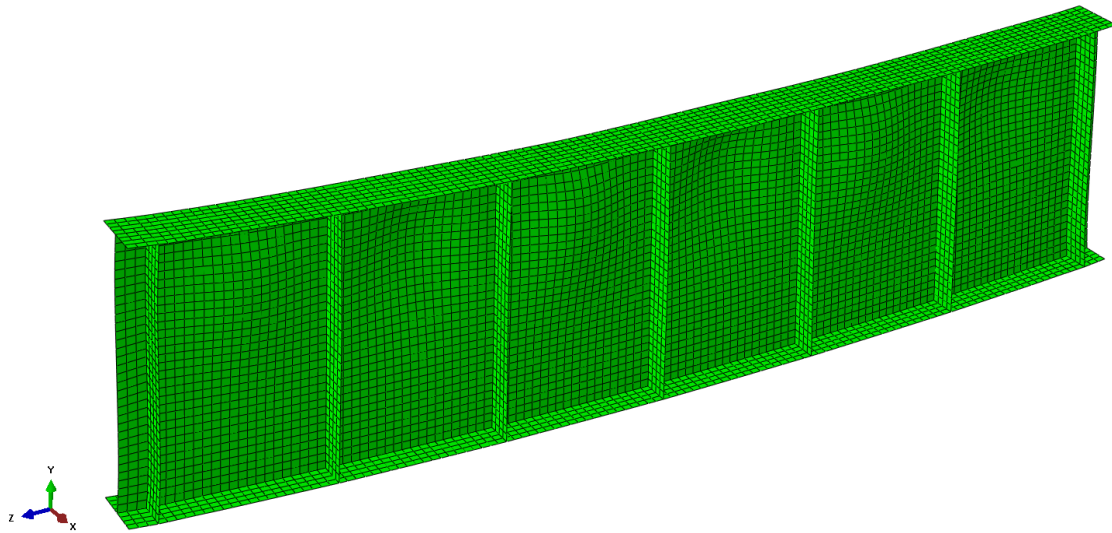
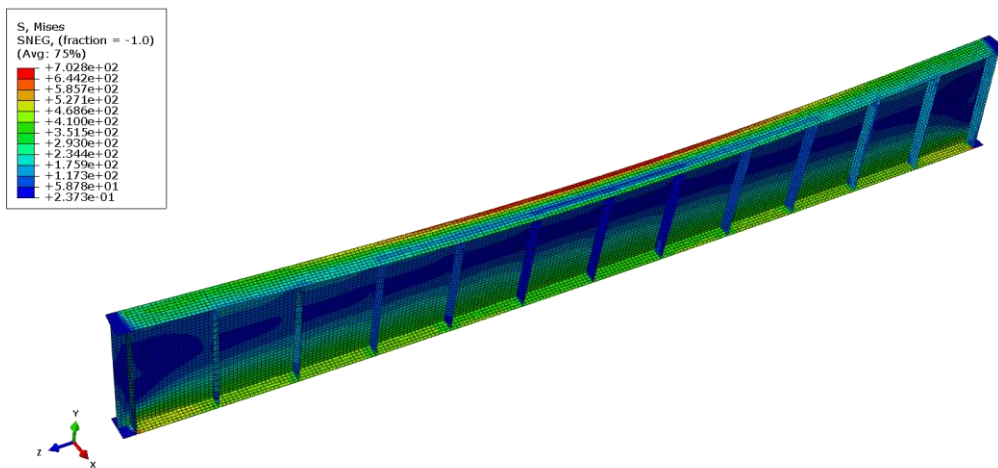


**Fig. 13:** Buckled/deformed shapes of a typical short IPG with stiffened slender web

(a) G1-12



(b) G1-20

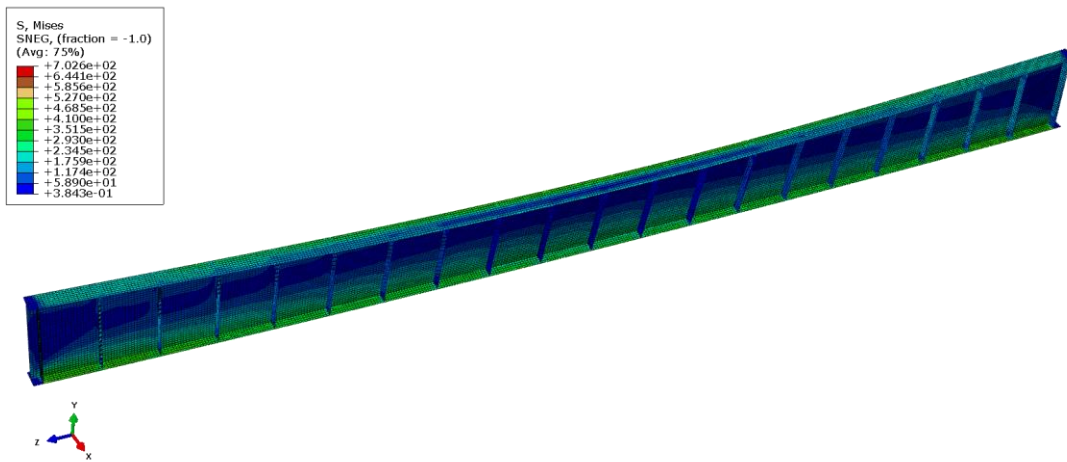


**Fig. 14:** Deformed shapes of long IPGs with stiffened slender web: (a) inelastic LTB and (b) elastic LTB

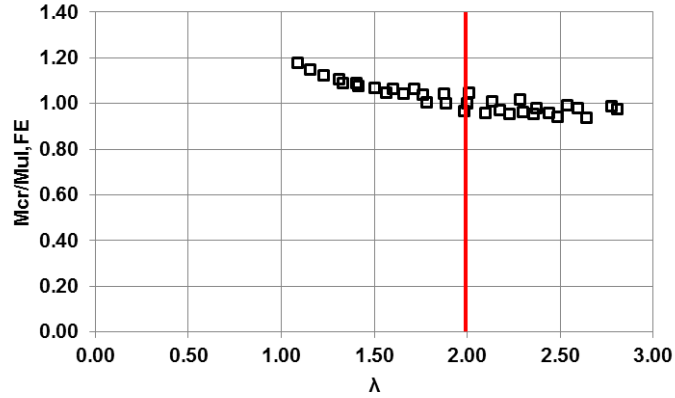


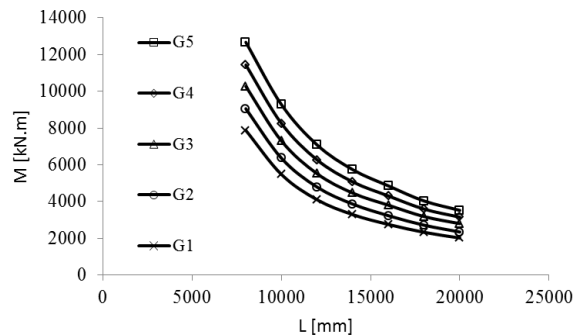
**Fig. 15:** Ratios of critical-to-ultimate FE strengths against the girders' slenderness for groups G1-G5

### 5.3 Effect of the effective radius of gyration for LTB ( $r_T$ )

Herein, the influence of the effective radius of gyration of the IPGs for LTB ( $r_T$ ), computed as the radius of gyration of the compression flange plus one-sixth of the web, is presented in **Fig. 16**. As can be seen, this figure provides  $M_{ul,FE}$  values and  $M_{ul,FE}/M_y$  ratios for groups G1-G5 against the unsupported length of the girders. Note that  $r_T$  varied from 92.6mm to 122.6mm, while  $S_{xc}$  was kept constant as previously presented in **Table 3**. Generally, the results of **Fig. 16(a)** point out that increasing the value of  $r_T$  raises the BM strengths of the IPGs. This confirms that the BM capacity grows by increasing the value of  $r_T$ , which conforms to the design model given by AISC [35]. From the relative values shown in **Fig. 16(b)**, it is clear that IPGs with larger  $r_T$  values can achieve higher flexural strengths compared with their elastic BM values. This is because increasing  $r_T$  values makes the flanges of the IPGs much stiffer with regard to their torsional capacities. Additionally, the

webs become stockier based on the strategy of keeping  $S_{xc}$  constant when the effect of  $r_T$  is evaluated (as the  $h_w/t_w$  ratios reduce by increasing  $r_T$  as seen in [Table 3](#)).

(a) Absolute moment values



(b) Relative moment values

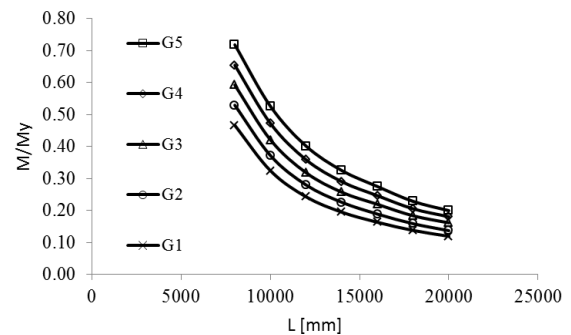


**Fig. 16:** Bending moment vs. laterally-unsupported length: (a)  $M_{ul,FE}$  and (b)  $M_{ul,FE} / M_y$  for Groups G1-G5

[Table 5](#) presents the ratios of  $(M_{Gn-L} / M_{G1-L})_{cr,FE}$ , which are the relative critical BM of each girder ( $M_{Gn-L}$ ) to its reference girder in G1 ( $M_{G1-L}$ ). The Variation of ratio between  $M_{ul,FE}$  values is also calculated and added to the table. Generally, the increase in the ratios of  $(M_{Gn-L} / M_{G1-L})_{cr,FE}$  and  $(M_{Gn-L} / M_{G1-L})_{ul,FE}$  is much greater than that of the  $r_T$  values (i.e.  $r_{Tn} / r_{T1}$  ratios). For example, between groups G5 and G1, it can be noticed that an increase of 32% ( $122.6/92.6=1.32$ ) takes place in  $r_T$  values. Considering  $M_{cr,FE}$  values, [Table 5](#) shows that  $(M_{G5-L} / M_{G1-L})_{cr,FE}$  ratios range from 1.70 (70% increase) to 1.74 (74% increase), with an average increase of 72%. With respect to  $M_{ul,FE}$  values, [Table 5](#) shows that  $(M_{G5-L} / M_{G1-L})_{ul,FE}$  values range from 1.61 (61% increase) and 1.75 (75% increase), with an average increase of 68%. For such 32% increase in the value of  $r_T$ , it can be noticed that the increase in  $M_{cr,FE}$  values is more than the increase in  $M_{ul,FE}$  values merely for relatively

short girders. Additionally, it is obvious that by increasing the unsupported length of the girders (i.e. the slenderness of the girder increases), the % increase in  $M_{cr,FE}$  values trivially decreases, while that of  $M_{ul,FE}$  values increases. The later observation regarding  $M_{ul,FE}$  values is simply because increasing the lateral stiffness (by increasing the  $r_T$  value) becomes much effective for the more slender girders. The comparisons for other groups show qualitatively the same trends. Overall, the effect of increasing the value of  $r_T$  looks positive and it might be considered for the efficient design of S690 transversely-stiffened IPGs to reduce the cost of such material.

**Table 5:** Variation ratios of  $r_T$ ,  $M_{cr,FE}$  and  $M_{ul,FE}$  between groups G2-G5 and the reference group G1

Radius of gyration ( $r_{Tn}/r_{T1}$ )				
-	1.08	1.16	1.24	1.32
Critical bending moments ( $M_{Gn-L}/M_{G1-L}$ ) <sub>cr,FE</sub>				
Span [m]	( $M_{G2}/M_{G1}$ )	( $M_{G3}/M_{G1}$ )	( $M_{G4}/M_{G1}$ )	( $M_{G5}/M_{G1}$ )
8	1.16	1.34	1.53	1.74
10	1.16	1.34	1.53	1.74
12	1.16	1.34	1.52	1.73
14	1.16	1.33	1.52	1.72
16	1.16	1.33	1.51	1.72
18	1.16	1.33	1.51	1.71
20	1.16	1.33	1.50	1.70
Ultimate bending moments ( $M_{Gn-L}/M_{G1-L}$ ) <sub>ul,FE</sub>				
8	1.15	1.30	1.45	1.61
10	1.16	1.33	1.51	1.69
12	1.17	1.35	1.53	1.73
14	1.17	1.36	1.54	1.75
16	1.17	1.38	1.56	1.76
18	1.17	1.37	1.54	1.73
20	1.16	1.39	1.56	1.75

The bending moment versus the vertical deflection ( $\delta$ ) curves obtained numerically for sample girders are additionally graphed in Fig. 17. In this figure, girders of 8m-span (Fig. 17(a)) and 14m-span (Fig. 17(b)) of the five groups have been considered. As can be noticed, there are no differences between the deflection profiles of the girders of different groups

considering each length. It is obvious that the relatively short girders (i.e.  $L_b$  of 8m) fail drastically, whereas those of long spans (i.e.  $L_b$  of 14m) fail gradually. Such gradual failure in large-span girders is attributed to the propagation of the second order torques from the onset of loading leading to this ductile manner [31]. As it is noticeable, the moment-deflection curves are formed from ascending and descending branches for the relatively short girders, while the curves are formed from ascending and strain hardening parts for long girders. For the girders with different lengths, the ascending portions for the curves extend linearly with nearly the same stiffness before the nonlinearity starts and propagates (which is more obvious in the larger girders) until reaching the maximum bending moments ( $M_{ul,FE}$ ). This means that the initial stiffness of the curves is hardly influenced by the change in the value of  $r_T$ .

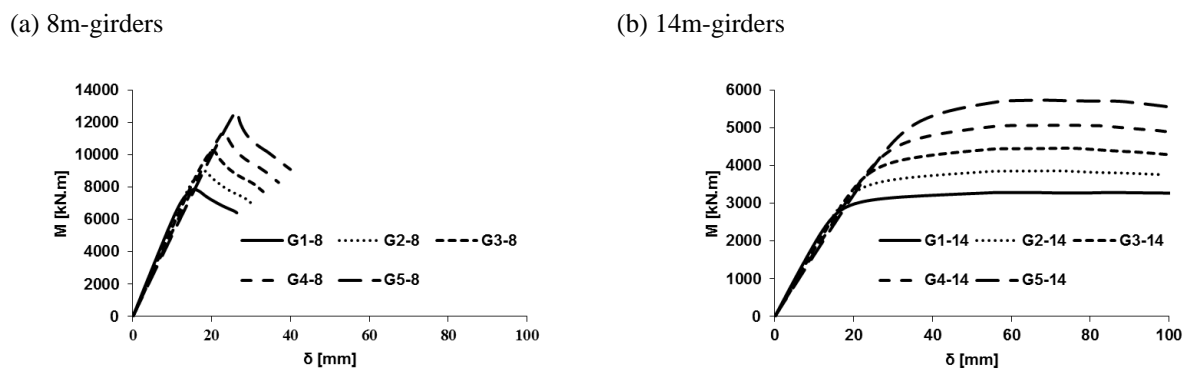


**Fig. 17:** Bending moment vs. mid-span deflection relationships for Groups G1-G5

#### 5.4 Effect of section modulus

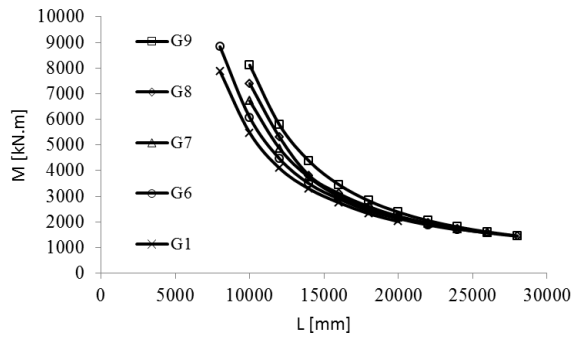
Herein, the results of the transversely-stiffened IPGs are provided to raise the awareness about the influence of the elastic section modulus referred to compression flange ( $S_{xc}$ ). The effect of  $S_{xc}$  could currently be examined by analysing the results of Groups G1 and G6-G9. The value of  $r_T$  of the girders of such groups was maintained constant ( $r_T = 92.6mm$ ), whilst the main variable was  $S_{xc}$  which had five different values as presented in Table 3. Generally,

the results indicated that increasing the value of  $S_{xc}$  (for a specific length) raises the maximum bending moments sustained by the IPGs as can be seen in Fig. 18(a), especially for relatively short girders. On the opposite, Fig. 18(b) indicates that  $M_{ul,FE}/M_y$  ratios decrease with the increase in  $S_{xc}$  values for the girders of the same length; especially for intermediate-length girders. This is simply attributed to the fact that the occurrence possibility of the LTB increases (and becomes more serious) when the variation between the section moduli of the two principle axes increases [31]. So, the girder with higher  $S_{xc}$  value becomes unable to reach higher strength compared with of the  $S_{xc}$  value of , increasing the Accordingly . $M_y$  girder provides less effective solution, with regard to material optimisation, when  $r_T$  value is kept the same.

In this subsection, the variation of ratio between  $M_{cr,FE}$  values of groups G6-G9 was also compared with the reference group G1, as provided in Table 6. Variation of ratio between  $M_{ul,FE}$  is also presented in the table as well as those of the section modulus ( $S_{xcn-L}/S_{xc1-L}$ ). Between groups G9 and G1, it can be noticed that the value of  $S_{xc}$  increased by 66% ( $44054778/26481270=1.66$ ). With respect to  $M_{cr,FE}$  values, Table 6 shows that  $(M_{G9-L}/M_{G1-L})_{cr,FE}$  values ranged from 1.51 (51%) and 1.35 (35% increase), with an average increase of 43%. On the other hand, with regard to  $M_{ul,FE}$  values, Table 6 shows that  $(M_{G9-L}/M_{G1-L})_{ul,FE}$  values range from 1.48 (48% increase) and 1.18 (18% increase), with an average increase of 33%. For this 66% increase in  $S_{xc}$  value, it is obvious that the increase is more visible for  $M_{cr,FE}$  values more than that of  $M_{ul,FE}$  values. The comparisons between the other groups and the reference group G1 show qualitatively the same results. Generally, for

any increase in the value of  $S_{xc}$ , it can be concluded that the increase is more evident for  $M_{cr,FE}$  values more than that of  $M_{ul,FE}$  values, but the % of increase is much lower than the increase in  $S_{xc}$ .

(a) Absolute moment values



(b) Relative moment values

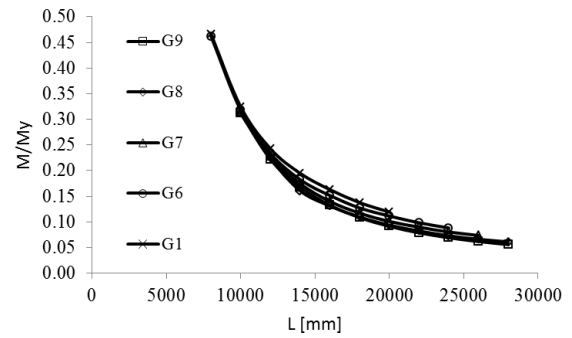


**Fig. 18:** Bending moment vs. laterally-unsupported length: (a)  $M_{ul,FE}$  and (b)  $M_{ul,FE} / M_y$  for Groups G1 and G6-G9

**Table 6:** Variation ratios of  $S_{xc}$ ,  $M_{cr,FE}$  and  $M_{ul,FE}$  between groups G6-G9 and the reference group G1

Radius of gyration ( $S_{xcn} / S_{xc1}$ )				
-	1.16	1.32	1.49	1.66
Critical bending moments ( $M_{Gn-L} / M_{G1-L}$ ) <sub>cr,FE</sub>				
Span [m]	( $M_{G6}/M_{G1}$ )	( $M_{G7}/M_{G1}$ )	( $M_{G8}/M_{G1}$ )	( $M_{G9}/M_{G1}$ )
10	1.12	1.24	1.37	1.51
12	1.11	1.22	1.35	1.48
14	1.10	1.21	1.32	1.44
16	1.09	1.19	1.30	1.41
18	1.08	1.18	1.27	1.38
20	1.08	1.16	1.25	1.35
Ultimate bending moments ( $M_{Gn-L} / M_{G1-L}$ ) <sub>ul,FE</sub>				
10	1.11	1.23	1.35	1.48
12	1.09	1.19	1.30	1.41
14	1.06	1.14	1.16	1.33
16	1.05	1.09	1.13	1.25
18	1.05	1.08	1.12	1.22
20	1.06	1.07	1.10	1.18

The bending moment versus mid-span vertical deflection relationships for sample girders (with span lengths of 10m and 14m) are presented herein in Fig. 19. Primarily, it is obvious that increasing the  $S_{xc}$  value raises the stiffness of the girders of both lengths. For the 10m span, the girders exhibit elastic relationships until about 80% of the ultimate moment followed with a nonlinear portion until reaching the ultimate moment. After that, the curves show descending failure behaviour which becomes steeper with the increase in value of  $S_{xc}$ . On the other hand, it can be recognised that the moment-deflection curves for the 14m girders are formed from ascending lines followed by unstable post peak parts of specimens of groups G8 and G9. Beyond the  $M_{ul,FE}$  value of these FE models (of G8 and G9), the load decreases moderately. On the opposite, girders of G1 and G6-G77 (with the less  $S_{xc}$  values relative to those of G8 and G9) are characterised by strain hardening parts.

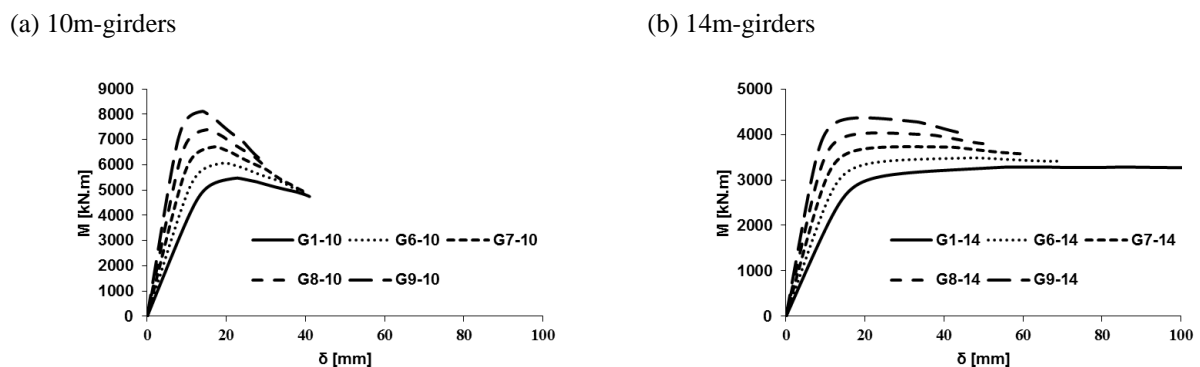


**Fig. 19:** Bending moment vs. mid-span deflection relationships for Groups G1 and G6-G9

## 5.5 Additional discussion

In this subsection, an emphasis is given to the variations in the values of both  $r_T$  and  $S_{xc}$ . Hence, girders of G5 and G9 are compared with each other with a sample span of 14m. Fig. 20 provides the moment-deflection relationships of girders G5-14 ( $M_{ul,FE}=5730 \text{ kN}\cdot\text{m}$ ) and G9-14 ( $M_{ul,FE}=4367 \text{ kN}\cdot\text{m}$ ), as well as that of the reference girder G1-14 ( $M_{ul,FE}=3284 \text{ kN}\cdot\text{m}$ ).

Note that the cross-sectional areas of girders G5-14 and G9-14 are 31200 and 38480mm<sup>2</sup>, respectively, while that of the reference girder is 30000 mm<sup>2</sup>. The statistics of these three representatives show that the cross-sectional areas of G5-14 and G9-14 are about 4% and 28% higher than that of G1-14. Furthermore, the strength increase was about 74% (G5-14) and 33% (G9-14) compared with that of G1-14. However, this increase in strength is accompanied by an increase in the vertical deflection of girder G5-14 (associated to  $M_{ul,FE}$  value) of about 14% and a deflection decrease of 67% for G9-14 relative to G1-14. So, it can be noticed that increasing  $r_t$  value (particularly by 33% in group G5 relative to G1) of the cross-section is much efficient than increasing the value of  $S_{xc}$  (which was about of 66% in group G9 relative to G1). Hence, designers should think in increasing the out-of-plane stiffness through increasing the  $r_t$  value as much as possible provided that the vertical deflection is less than the allowed codified limits, rather than increasing the value of  $S_{xc}$ . This is because increasing  $S_{xc}$  in turn increases considerably the cross-sectional area of girders formed from S690 (see Table 3), hence the material cost raises. By following this recommendation, grade S690 may be utilised efficiently in structural engineering applications.

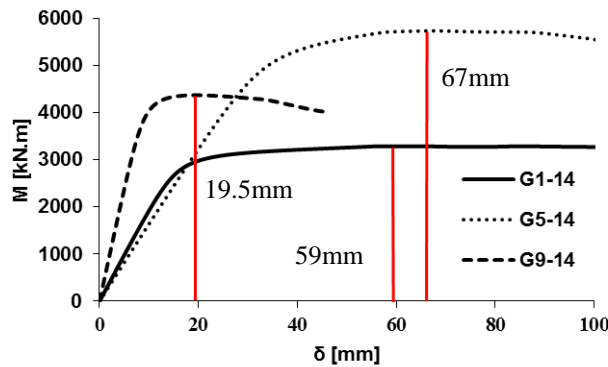


**Fig. 20:** Comparison between girders of Groups G1, G5 and G9 with a span length of 14m

## 6. COMPARISONS WITH DESIGN MODELS

This section provides the comparison between the flexural strengths ( $M_{ul,FE}$ ) of the current girders and the unfactored predictions given by the specifications of ANSI/AISC 360-16 [35] ( $M_{n,AISC}$ ), EN1993-1-12 [37] ( $M_{n,EC3}$ ) and AS4100 [38] ( $M_{n,AS}$ ). Generally, all these design manuals [35-38] reduce the cross-sectional capacities of the girders by a slenderness reduction factor to obtain their LTB strengths. Herein, the design models of these specifications are summarised followed by the comparisons. Then, a suggested design model is provided at the end.

### 6.1 ANSI/AISC 360-16 [35]

Section F5 [35] was used to calculate the flexural strengths of the current girders, which are bent about their major-axes. This is because this section applies to doubly-symmetric I-shaped members with slender webs welded to the mid-width of the flanges. In this design model, the nominal flexural strength ( $M_{n,AISC}$ ) is the lowest value obtained according to the limit states of (1) compression flange yielding, (2) LTB, (3) compression flange local buckling and (4) tension flange yielding. Because the current girders are of thick (i.e. compact) flanges, the limit state of the compression flange local buckling is eliminated. Additionally, the compression flange yielding limit state is to be excluded because all of the current girders failed by LTB. Accordingly, the nominal flexural strength,  $M_{n,AISC}$ , shall be the lowest value obtained according to the limit states of LTB and tension flange yielding (if  $S_{xt} < S_{xc}$ ), where  $S_{xt}$  and  $S_{xc}$  are the elastic section moduli referred to tension and compression flanges, respectively. However, for the case of the current doubly-symmetric girders failing, the values of  $S_{xt}$  and  $S_{xc}$  are equal. Hence, the design strength according to AISC [35] is finally given by Eq. F5-2 [35], as follows:

$$M_{n,AISC} = R_{pg} F_{cr} S_{xc} \quad (1)$$

where  $R_{pg}$  is the bending strength reduction factor, calculated as:

$$R_{pg} = 1 - \frac{a_w}{1200 + 300a_w} \left( \frac{h_c}{t_w} - 5.7 \sqrt{\frac{E}{f_y}} \right) \leq 1.0 \quad \text{and} \quad a_w = \frac{h_c t_w}{b_{fc} t_{fc}} \quad (2)$$

where  $h_c$  is twice the distance from the centroid to the inside face of the compression flange when welds are used in case of built-up sections,  $b_{fc}$  and  $t_{fc}$  are the width and thickness of the compression flange, respectively, and  $t_w$  is the thickness of the web. Additionally, the critical stress ( $F_{cr}$ ) is computed as:

$$F_{cr} = \begin{cases} C_b \left[ f_y - (0.3F_y) \left( \frac{L_b - L_p}{L_r - L_p} \right) \right] \leq f_y & : L_p < L_b \leq L_r \\ \frac{C_b \pi^2 E}{\left( \frac{L_b}{r_t} \right)^2} \leq f_y & : L_b > L_r \end{cases} \quad (3)$$

where  $L_p = 1.1r_t \sqrt{\frac{E}{F_y}}$ ,  $L_r = \pi r_t \sqrt{\frac{E}{0.7F_y}}$ ,  $r_t$  is the radius of gyration of the flange components

as defined earlier in this paper;  $r_t$  and  $C_b$  is the moment modification factor taken herein as unity for the case of uniform bending moment.

## 6.2 EN 1993-1-12 [37]

EN 1993-1-12 [37] provides the additional rules which extend the use of EN 1993-1-1 [36] up to steel grades S700. Nevertheless, EN1993-1-12 [37] has not provided additional rules regarding the design of uniform flexural members to those given in clause 6.3.2 of EN 1993-

1-1 [36]. Accordingly, the rules of EC3 [36] stand for the current girders formed from S690 [25]. Hence, the unfactored design resistance ( $M_{n,EC3}$ ) of such laterally-unsupported girder is given as:

$$M_{n,EC3} = \chi_{LT} W_y f_y \quad (4)$$

Where  $W_y = W_{eff,y}$ , in which  $W_{eff,y}$  is the effective section modulus for slender (Class 4) sections and  $\chi_{LT}$  is the reduction factor for LTB which is given in Clause 6.3.2.2 [36] as:

$$\chi_{LT} = \frac{1}{\Phi_{LT} + \sqrt{\Phi_{LT}^2 - \bar{\lambda}_{LT}^2}} \leq 1.0 \quad (5)$$

where  $\Phi_{LT}$  is a value given by EC3 [36] to determine  $\chi_{LT}$ , and it is computed as:

$$\Phi_{LT} = 0.5 \left( 1 + \alpha_{LT} (\bar{\lambda}_{LT} - \bar{\lambda}_{LT,0}) + \beta \bar{\lambda}_{LT}^2 \right) \quad \text{with} \quad \bar{\lambda}_{LT} = \sqrt{\frac{W_y f_y}{M_{cr,LTB}}} \quad (6)$$

where  $M_{cr,LTB}$  is the elastic critical moment for LTB which is based upon the gross sectional properties and takes the loading conditions into account, the real moment distribution and the lateral restraint. It is interesting to note that parameters  $\bar{\lambda}_{LT,0}$  and  $\beta$  have two values for each, which depends on the clause used in the calculations [36]. If the general case (specified in Clause 6.3.2.2) is used, parameters  $\bar{\lambda}_{LT,0}$  and  $\beta$  are taken as 0.2 and 1.0, respectively. On the other hand, if Clause 6.3.2.3 is utilised (which applies for the special case of welded sections), the parameters are taken as  $\bar{\lambda}_{LT,0} = 0.4$  and  $\beta = 0.75$ . Herein, both clauses [36] have been considered. Hence, the strengths are termed as  $M_{n,EC3,Gen}$  and  $M_{n,EC3,WS}$  when the

general case of the LTB (Clause 6.3.2.2) and LTB of welded sections (Clause 6.3.2.3) are used, respectively. Note that  $\alpha_{LT}$  is the imperfection factor of buckling curve "d", and it is taken as 0.76 for welded open sections.

### 6.3 AS4100 [38]

As stated by AS4100 [38] (in Clause 5.6.1.1), the strength of a laterally-unsupported steel girder subjected to major-axis bending, under uniform bending, is given as:

$$M_{n,AS} = \alpha_s M_p \leq M_p \quad (7)$$

$$\alpha_s = 0.6 \left[ \sqrt{\bar{\lambda}_{LT}^4 + 3} - \bar{\lambda}_{LT}^2 \right] \quad (8)$$

where  $\alpha_s$  is the slenderness reduction factor,  $M_p$  is the plastic bending moment of the girder's cross-section, the slenderness is given by  $\bar{\lambda}_{LT} = \sqrt{M_y / M_{cr,LTB}}$  and  $M_y$  represents the cross-sectional resistance moment of the girder.

### 6.4 Comparisons with above design models

Herein, the comparisons between the FE bending strengths ( $M_{ul,FE}$ ) and the predictions of different codes ( $M_{Code}$ ) [35-38] are provided. Fig. 21 displays  $M_{ul,FE} / M_{Code}$  ratios against the slenderness of the girders ( $\lambda_{LT}$ ), which is calculated according to EC3 [36]. As can be noticed, the design models of AISC [35], EC3-General [36] and AS4100 [38] provide safe predictions, while that of EC3-WS [36] shows unsafe strengths for girders with  $\lambda_{LT} > 2.0$ . It can also be recognised that AISC [35] provides highly conservative predictions, from which the  $M_{ul,FE} / M_{n,AISC}$  ratios may reach 1.8. This is attributed to the implicit use of  $J = 0.0$  in Section F5. AISC [35] intentionally neglects the torsional constant ( $J$ ) in the calculations, as

given in Commentary F5 [35], to account for the influence of web distortional flexibility on the LTB resistance for I-section members with slender webs. To ensure that this is the main reason for the highly conservative results of AISC [35],  $J$  was taken zero in the calculations of the EC3 [36-37] and AS4100 [38]. The results of this check is provided in Fig. A of Appendix A, from which the Specifications [36-38] show similar (and even higher) very conservative predictions to that of AISC [35]. Accordingly, this assumption should be revised as the IPGs formed by closely-spaced transversely stiffeners do not suffer from web distortion.

The statistics with respect to the maximum (Max), minimum (Min), average (Ave) and standard deviation (SD) of  $M_{ul,FE} / M_{Code}$  ratios are provided in Table 7. Based on such statistics, it can be recognised that the predictions of AS4100 [38] are the most suitable predictions with the least average ratio of 1.24, without unsafe predictions (i.e. Min. of 1.02). However, additional enhancement could be made to the design models to reach better predictions. This is done in the next subsection.

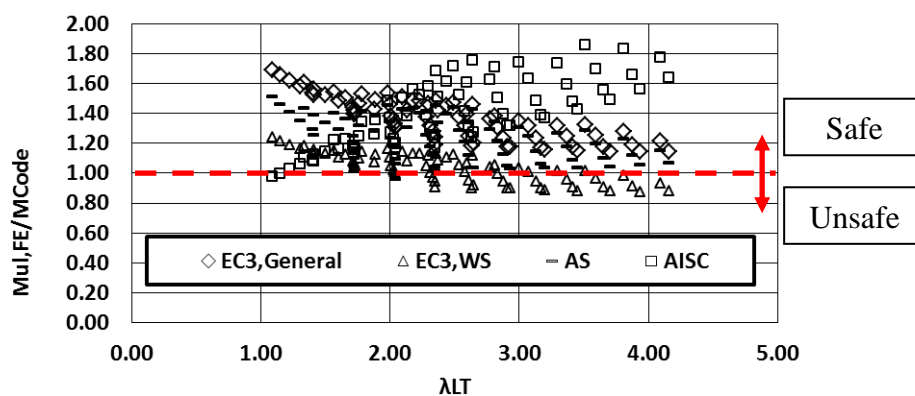


**Fig. 21:** Comparison between FE strengths and code predictions [35-38]

**Table 7:** Statistics of FE-to-code prediction ratios ( $M_{ul,FE} / M_{Code}$ )

Statistics	AISC [35]	EC3 [36] – General (Buckling curve "d")	EC3 [36] – WS (Buckling curve "d")	AS4100 [38]	EC3 [36] – General (Buckling curve "a")
Max	1.86	1.69	1.24	1.51	1.22
Min	0.98	1.14	0.88	1.02	0.97
Ave	1.39	1.37	1.04	1.24	1.10
SD	0.224	0.142	0.096	0.141	0.068

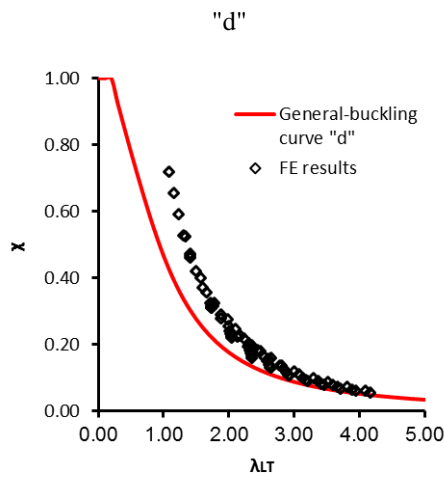
## 6.5 Suggested design model

In this subsection, a modification for EC3 design model [36] is suggested. To do so, the reduction factor for LTB ( $\chi_{FE}$ ) is calculated based on the FE strengths and the cross-section resistances as  $\chi_{FE} = M_{ul,FE} / M_y$ . The relationship between the codified  $\chi_{LT}$  and the slenderness of the girders were then drawn with respect to certain buckling curves, and  $\chi_{FE}$  values for the girders were added to these relationships. These relationships can be seen in Fig. 22. Graphs (a) and (b) of this figure were obtained by using the original design models of EC3 [36], which adopt buckling curve "d" as discussed earlier in Section 6.2. As it is well known, this buckling curve is the most conservative among curves recommended in EC3 [36]. Hence, the method of equivalent welded sections, which is already unsafe by using this curve, cannot benefit from enhancing such buckling curve. On the opposite, as the LTB general method (Clause 6.3.2.2) is highly conservative, enhancing the buckling curve may be beneficial in providing efficient design. Accordingly, the lower graph in Fig. 22 presents the results after upgrading the buckling curve to "a". From this figure and the statistics shown in Table 7, it can be noticed that using the general method (Clause 6.3.2.2) in predicting the LTB strengths with upgraded buckling curve "a" provides the best predictor for the bending strengths of the transversely-stiffened IPGs formed from S690. Hence, it is currently recommended for design. Note that this suggested strength conforms to the previous investigation by Somodi and Kövesdi [39] on the flexure buckling of HSS members. In such investigation, buckling curves for steels of S420 and S960 were upgraded by using curves

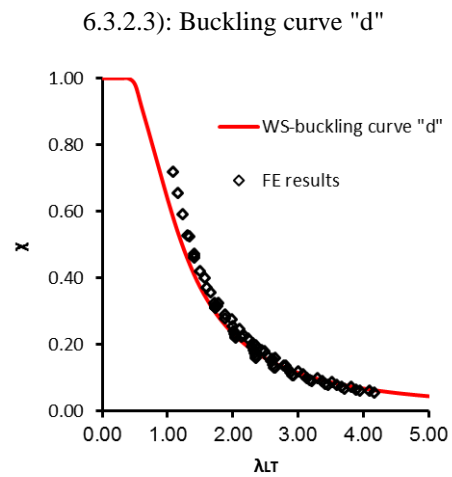
with smaller imperfection factors ( $\alpha_{LT}$ ) [36]. According to Somodi and Kövesdi [39], the buckling resistances for above mentioned steel grades were always higher than the recommended buckling curve in EN 1993-1-1 [36]. This is principally credited to the fact that the amplitudes of residual stress have minor effect on the behaviour of HSS members relative to their yield strengths than their effects on NSS structures [40].

On the other hand, the AS4100 [38] design model could be enhanced by applying the Ayrton-Perry formulation (adopted by EC3 [36] and given here by Eq. 5) instead of that currently adopted (Eq. 8). This makes it approaches the design model of EC3 [36], as both specifications use a reduction factor to the cross-sectional capacity. Additionally, as discussed in Section 6.4, the assumption of neglecting torsional constant ( $J$ ) in the calculations by AISC [35] design model should not be adopted. By doing so, this design model would be enhanced because the IPGs formed by closely-spaced transversely stiffeners do not suffer from web distortion. However, a modified design model using AISC [35] could be suggested in future publication. This is because this design specification computes the strength capacity of the girder depending on the unsupported lengths ( $L_p$  and  $L_r$ ). Hence, the precise design must the significant difference between this method (AISC [35]) and what is followed in the other codes (EC3 [36] and AS4100 [38]) take into account. More importantly, the current assessment of the AISC [35] design model ignored three limit states (refer back to Section 6.1). So, suggesting a modified version of this design model requires additional parametric analyses to provide the different failure modes currently ignored; namely (1) compression flange yielding, (2) compression flange local buckling and (3) tension flange yielding.

(a) General method (Clause 6.3.2.2): Buckling curve "d"



(b) Method of equivalent welded sections (Clause 6.3.2.3): Buckling curve "d"



(c) General method (Clause 6.3.2.2): Buckling curve "a" – recommended method

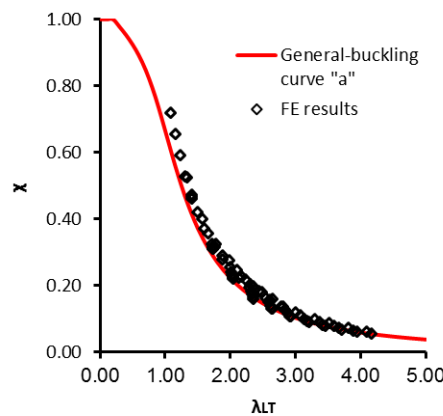


**Fig. 22:**  $\chi - \lambda_{LT}$  relationships calculated by (a) the general method (Clause 6.3.2.2), (b) the method of equivalent welded sections (Clause 6.3.2.3) [36] and (c) the recommended curve

## 7. CONCLUSIONS

This paper explored the lateral-torsional buckling (LTB) strength and behaviour of transversely-stiffened I-section plate girders with slender webs, for bridge construction. These girders were built up from S690 high-strength steel (HSS), which has not yet been examined in the literature. On the basis of this finite element (FE) investigation, the following conclusions can be summarised:

1. The behaviour of the HSS S690 can successfully be obtained by using the elastic-perfect plastic model with strain hardening.
2. A girder slenderness parameter of 2.0 was found as the limiting inelastic LTB, from which girders beyond this limit cannot benefit from using the HSS material.
3. Increasing the effective radius of gyration for LTB ( $r_T$ ) of the cross-section was found positively to raise the bending strength of the current IPGs, and hence it might be increased for the efficient design of the transversely-stiffened IPGs with slender webs.
4. The results showed that increasing the section modulus ( $S_{xc}$ ) of the IPGs raises the bending strength of the girders. Nevertheless, for any increase in the value of  $S_{xc}$ , the % of increase in the ultimate moments is much lower than the increase in the value of  $S_{xc}$ .
5. Using the AISC [35] design model was found to yield highly conservative results because it neglects the torsional constant ( $J$ ) in the calculations. Hence, this assumption should be revised to enhance the design prediction of AISC [35] as the IPGs formed by closely-spaced transversely stiffeners do not suffer from web distortion.
6. The best prediction of the bending strengths of the current transversely-stiffened IPGs with slender webs was obtained by utilising the design model of AS4100 [38] compared with those attained by AISC [35] and EC3 [37]. However, it is still conservative and could be enhanced by adopting the Ayrton-Perry formulation (adopted by EC3 [36] and given herein by Eq. 5) instead of that currently adopted slenderness reduction factor (Eq. 8).
7. Based on the previous point, a modification for the design model recommended by EC3 [36] has been suggested considering the LTB general method (Clause 6.3.2.2).

This modification was made by upgrading the buckling curve "a" instead of "d". Hence, it is currently recommended for design.

8. The results of this paper encourage designers to increase the  $r_T$  value as much as possible provided that the vertical deflection is less than the allowed codified limits. This is instead of increasing the value of  $S_{xc}$  which in turn increases the cross-sectional area of girders formed from S690. By doing so, steel S690 may be utilised efficiently in the structural engineering applications.

## ACKNOWLEDGEMENT

This study is supported by Scientific Innovation Group for Youths of Sichuan Province (No. 2019JDTD0017), and such support is appreciated greatly by the author.

## REFERENCES

- [1] Gkantou, M., Theofanous, M., Baniotopoulos, C., "Plastic Design of Hot-Finished High Strength Steel Continuous Beams", *Thin-Walled Structures*, Vol. 133, pp. 85-95, 2018.
- [2] "Behavior of High Strength Concrete Encased Steel Composite Stub Columns with C130 Concrete and S690 Steel", *Engineering Structures*, Vol. 200, 109743, 2019
- [3] Gogou, E., "Use of High Strength Steel Grades for Economical Bridge Design", Master thesis study, Delft University of Technology Iv-Infra, Amsterdam, 2012.
- [4] Li, G.-Q., Lyu, H., Zhang, C., "Post-Fire Mechanical Properties of High Strength Q690 Structural Steel ", *Journal of Constructional Steel Research*, Vol. 132, pp. 108-116, 2017.
- [5] Nidheesh, P.V., Kumar, M.S., "An Overview of Environmental Sustainability in Cement and Steel Production", *Journal of Cleaner Production*, Vol. 231, pp. 856-871, 2019.

- [6] WSA: World Steel Association, "The Three Rs of Sustainable Steel", World Steel Association, 2010.
- [7] Zhang, L., Wang, F., Liang, Y., Zhao, O., "Experimental and numerical studies of press-braked S690 high strength steel channel section beams", *Thin-Walled Structures*, <https://doi.org/10.1016/j.tws.2019.106499>.
- [8] Sun, Y., He, A., Liang, Y., Zhao, O., "In-plane Bending Behaviour and Capacities of S690 High Strength Steel Welded I-Section Beams", *Journal of Constructional Steel Research*, Vol. 162, 105741, 2019.
- [9] Wang, F., Zhao, O., Young, B., "Flexural behaviour and strengths of press-braked S960 ultra-high strength steel channel section beams", *Engineering Structures*, Vol. 200, 109735, 2019.
- [10] Sun, Y., Liang, Y., Zhao, O., "Testing, numerical modelling and design of S690 high strength steel welded I-section stub columns", *Journal of Constructional Steel Research*, Vol. 159, pp. 521-533, 2019.
- [11] Zhang, L., Wang, F., Liang, Y., Zhao, O., "Press-braked S690 high strength steel equal-leg angle and plain channel section stub columns: Testing, numerical simulation and design", *Engineering Structures*, Vol. 201, 109764, 2019.
- [12] Kalkan, L., Buyukkaragoz, A., "A numerical and analytical study on distortional buckling of doubly-symmetric steel I-beams", *Journal of Constructional Steel Research*, Vol. 70, pp. 289-297, 2012.
- [13] Höglund, T., "Design of Thin Plate I Girders in Shear and Bending", *R Inst Technol Bull* No. 94, Stockholm, 1973.
- [14] Chacón, R., Mirambell, E., Real, E., "Transversally stiffened plate girders subjected to patch loading. Part 1. Preliminary study", *Journal of Constructional Steel Research*, Vol. 80, pp. 483-491, 2013.

- [15] Nguyen, C.T., Moon, J., Le, V.N., and Lee, H., "Lateral-Torsional Buckling of I-Girders with Discrete Torsional Bracings", *Journal of Constructional Steel Research*, Vol. 66, pp. 170-177, 2010.
- [16] Alinia MM, Shakiba, M and SAA, Habashi HR., "Shear Failure Characteristics of Steel Plate Girders", *Thin-Walled Structures*, Vol. 47, pp. 1498-1506, 2009.
- [17] Chacón, R., Mirambell, E., Real, E., "Transversally stiffened plate girders subjected to patch loading. Part 1. Additional numerical study and design proposal", *Journal of Constructional Steel Research*, Vol. 80, pp. 492-504, 2013.
- [18] Hassanein, M.F., Kharoob O.F., El Hadidy, A.M., "Lateral-Torsional Buckling of Hollow Tubular Flange Plate Girders with Slender Stiffened Webs", *Thin-Walled Structures*, Vol. 65, pp. 49-61, 2013.
- [19] Bradford, M.A., Liu, X., "Flexural-Torsional Buckling of High-Strength Steel Beams", *Journal of Constructional Steel Research*, Vol. 124, pp. 122-131, 2016.
- [20] Elkawas, A.A., Hassanein, M.F., Elchalakani, M., "Lateral-Torsional Buckling Strength and Behaviour of High-Strength Steel Corrugated Web Girders for Bridge Construction", *Thin-Walled Structures*, Vol. 122, pp. 112-123, 2018.
- [21] Shao, Y.-B., Zhang, Y.-M., Hassanein, M.F., "Strength and Behaviour of Laterally-Unrestrained S690 High-Strength Steel Hybrid Girders with Corrugated Webs", *Thin-Walled Structures*, Vol. 150, 106688, 2020.
- [22] Liang, Y., Zhao, O., Long, Y., Gardner, L., "Stainless Steel Channel Sections under Combined Compression and Minor Axis Bending - part 1: experimental study and numerical modelling", *Journal of Constructional Steel Research*, Vol. 152, pp. 154-161, 2019.
- [23] Saliba, N., Gardner, L., "Cross-Section Stability of Lean Duplex Stainless Steel Welded I-Sections", *Journal of Constructional Steel Research*, Vol. 80, 1-14, 2013.

- [24] Gardner, L., "Stability and Design of Stainless Steel Structures - Review and Outlook", *Thin-Walled Structures*, Vol. 141, pp. 208-216, 2019.
- [25] Jönsson, J., Stan, T.-C., "European Column Buckling Curves and Finite Element Modelling Including High Strength Steels", *Journal of Constructional Steel Research*, Vol. 128, pp. 136-151, 2017.
- [26] Bijlaard, F., Feldmann, M., Naumes, J., Müller, C., Sedlacek, G., "Consistency of Equivalent Geometric Imperfections Used in Design and the Tolerances for Geometric Imperfections Used in Execution", Report CEN/TC250-CEN/TC135-Liaison, N1721, February 2010.
- [27] EN 1090–2:2008, "Execution of Steel Structures and Aluminium Structures - Part 2: Technical Requirements for Steel Structures", CEN - European committee for Standardization, Brussels (Belgium), 2008.
- [28] Hassanein, M.F., Kharoob O.F., "Shear Capacity of Stiffened Plate Girders with Compression Tubular Flanges and Slender Webs", *Thin-Walled Structures*, Vol. 70, pp. 81-92, 2013.
- [29] Hassanein, M.F., Silvestre N., "Flexural Behaviour of Lean Duplex Stainless Steel Girders with Slender Unstiffened Webs", *Journal of Constructional Steel Research*, Vol. 85, pp. 12-23, 2013.
- [30] EN 1993-1-5, "Eurocode 3: Design of steel structures - Part 1-5: Plated structural elements", CEN, 2007.
- [31] Timoshenko, S.P., Gere, J.M., "Theory of Elastic Stability", McGraw-Hill, London, 2nd edition, 1961.
- [32] Dibley, J.E., "Lateral Torsional Buckling of I-Sections in Grade 55 Steel", *ICE Proceedings*, Vol. 43 (4), pp. 599-627, 1969.

- [33] Dux, P.F., Kitipornchai, S., "Inelastic Beam Buckling Experiments", Journal of Constructional Steel Research, Vol. 3(1), pp. 3-9, 1983.
- [34] White, D.W., Jung, S., "Effect of Web Distortion on the Buckling Strength of Noncomposite Discretely-Braced Steel I-Section Members", Engineering Structures, Vol. 29, pp. 1872-1888, 2007.
- [35] ANSI/AISC 360-16, "Specification for Structural Steel Buildings", American Institute of Steel Construction (AISC), Chicago, Illinois 60601-6204, 2016.
- [36] EN 1993-1-1. Eurocode 3: Design of steel structures - Part 1-1: General rules and rules for buildings. CEN; 2004.
- [37] EN 1993-1-12, "Eurocode 3: Design of steel structures - Part 1-12: Additional rules for the extension of EN 1993 up to steel grades S 700", CEN, 2009.
- [38] Standards Association of Australia. AS4100 steel structures. Sydney, Australia, 1998.
- [39] Somodi, B., Kövesdi, B. "Flexural buckling resistance of welded HSS box section members", Thin-Walled Structures, Vol. 119, pp. 266-281, 2017.
- [40] Somodi, B., Kövesdi, B., "Residual Stress Measurements on Cold-Formed HSS Hollow Section Columns", Journal of Constructional Steel Research, Vol. 128, pp. 706-720, 2017.

**APPENDIX A:** FE strengths and code predictions [35-38] considering  $J = 0.0$

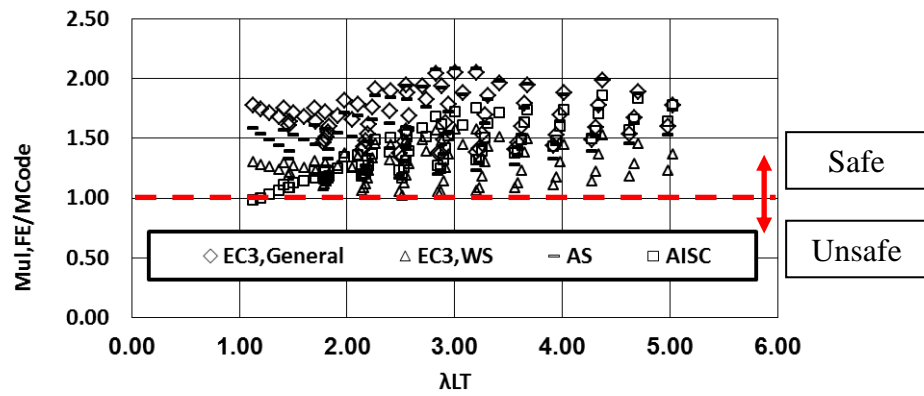


**Fig. A:** Comparison between FE strengths and code predictions [35-38] assuming that

$$J = 0.0$$